

Determinant Estimation under Memory Constraints and Neural Scaling Laws

Siavash Ameli¹, Chris van der Heide², Liam Hodgkinson³, Fred Roosta⁴, and Michael W. Mahoney⁵

¹*ICSI and Department of Statistics, University of California, Berkeley*
sameli@berkeley.edu

²*Dept. of Electrical and Electronic Engineering, University of Melbourne*
chris.vdh@gmail.com

³*School of Mathematics and Statistics, University of Melbourne*
lhodgkinson@unimelb.edu.au

⁴*CIRES and School of Mathematics and Physics, University of Queensland*
fred.roosta@uq.edu.au

⁵*ICSI, LBNL, and Department of Statistics, University of California, Berkeley*
mmahoney@stat.berkeley.edu

Abstract

Calculating or accurately estimating log-determinants of large positive semi-definite matrices is of fundamental importance in many machine learning tasks. While its cubic computational complexity can already be prohibitive, in modern applications, even storing the matrices themselves can pose a memory bottleneck. To address this, we derive a novel hierarchical algorithm based on block-wise computation of the LDL decomposition for large-scale log-determinant calculation in memory-constrained settings. In extreme cases where matrices are highly ill-conditioned, accurately computing the full matrix itself may be infeasible. This is particularly relevant when considering kernel matrices at scale, including the empirical Neural Tangent Kernel (NTK) of neural networks trained on large datasets. Under the assumption of neural scaling laws in the test error, we show that the ratio of pseudo-determinants satisfies a power-law relationship, allowing us to derive corresponding scaling laws. This enables accurate estimation of NTK log-determinants from a tiny fraction of the full dataset; in our experiments, this results in a $\sim 100,000\times$ speedup with improved accuracy over competing approximations. Using these techniques, we successfully estimate log-determinants for dense matrices of extreme sizes, which were previously deemed intractable and inaccessible due to their enormous scale and computational demands.

1 Introduction

Many quantities of interest in machine learning require accurate estimation of the log-(pseudo-)determinant of large dense positive (semi-)definite matrices, often indexed by some number of datapoints. These quantities arise in a number of tasks, including training Gaussian processes (GPs) and other kernel-based methods (Wang et al., 2019), graphical models (Rue & Held, 2005), determinantal point processes (Kulesza et al., 2012), and model comparison and selection techniques (Hodgkinson et al., 2023b). Problems where the calculation cannot be avoided can often be reduced to computing a volume form, which is the case for tasks in statistical mechanics (Mézard & Montanari, 2009) or Bayesian computation (Gelman et al., 2013), or applications of the Karlin-McGregor theorem (Karlin & McGregor, 1959) including determinantal point processes. Similarly, when training GPs via empirical Bayes (Rasmussen & Williams, 2006), the log-determinant term is the most difficult to compute. In many applications, these matrices are not only dense but highly ill-conditioned. This renders methods that leverage sparsity inappropriate and makes accurate estimation of small eigenvalues crucial,

since errors in these small values are magnified at log-scale. Much of the research focus has concentrated on approximation techniques that ameliorate the cubic computational complexity of these log-determinant calculations. Methods leveraging stochastic expansions that rely upon matrix-vector multiplications—such as Lanczos-based methods (Ubaru et al., 2017)—have been particularly successful, yielding approximate methods that scale linearly (Dong et al., 2017), and methods leveraging Taylor’s expansions (Fitzsimons et al., 2017) have also been proposed. However, accuracy can suffer when they encounter common ill-conditioning pathologies. Crucially, time complexity isn’t the only bottleneck at play: large-scale matrices found in modern applications often hit the memory wall before computational cost becomes an issue (Gholami et al., 2024).

Recently, the empirical Neural Tangent Kernel (NTK) has become a prominent theoretical and practical tool for studying the behavior of neural networks both during training and at inference (Novak et al., 2022). The Gram matrix associated with the NTK has been used in lazy training (Chizat et al., 2019) and shows promise as a tool to obtain uncertainty quantification estimates (Immer et al., 2021). Its log-determinant—highly sensitive to small eigenvalues—has also received recent attention, both as a quantity of interest in model selection techniques that rely upon marginal likelihood approximation (Immer et al., 2023; Hodgkinson et al., 2023b) and as a way to quantify the complexity of a learning problem (Vakili et al., 2022). Similarly, both the NTK log-determinant and closely related quantities have recently appeared in quantification of generalization error via PAC-Bayes bounds (Hodgkinson et al., 2023c; Kim et al., 2023). While several approximations have been proposed (Mohamadi et al., 2023), convergence has only been shown in spectral norm, so they can only be expected to capture the overall behavior of the full NTK.

In practice, computing the log-determinant of the empirical NTK’s Gram matrix is a formidable task: besides suffering from the pathologies that ill-conditioned matrices are subject to at scale, the NTK appears to have its own peculiarities that make the problem particularly challenging. Indeed, *the task is considered so impenetrable as to be universally avoided*, since the NTK corresponding to most relevant datasets cannot be stored in memory. For example, storing the NTK corresponding to the relatively small MNIST dataset requires 2.9 terabytes of memory. The equivalent object for ImageNet-1k requires 13.1 exabytes, an order of magnitude larger than CERN’s current data storage capacity (Smith, 2023). While it is appealing to consider only a small subset of the training dataset when considering such approximations, these estimates for the log-determinant can incur significant bias. Furthermore, we will find that leading approaches for dealing with log-determinants of empirical NTK Gram matrices using sketching and other Monte Carlo approximations tend to be highly inaccurate.

Contributions. The central contributions of this work address the issues faced when computing log-determinants of large matrices. We are primarily interested in matrices that cannot fit into memory. To compute an accurate baseline, we derive MEMDET, a memory-constrained algorithm for determinant computation. This facilitates exact calculation of log-determinants of NTK Gram matrices corresponding to neural networks with several million parameters, for the first time on datasets this large. We then provide a novel approximation technique based on the scaling behavior of a wide class of kernel matrices, by appealing to *neural scaling laws*. Scaling laws have played a prominent role in machine learning theory and practice, providing insight into the asymptotic behavior of generalization error (Li et al., 2023; Vakili et al., 2022), as well as guidance for compute-optimal resource allocation when deploying deep learning models at scale (Kaplan et al., 2020; Hoffmann et al., 2022). Specifically,

- we derive a hierarchical memory-constrained algorithm for large-scale computation of log-determinants, which we name MEMDET;
- under mild assumptions, we derive scaling laws for the ratio of pseudo-determinants of kernel matrices containing different subsets of the same dataset, enabling both a corresponding law of large numbers and central limit theorem for normalized log-determinants;
- leveraging these scaling laws, we propose FLODANCE, a novel algorithm for accurate extrapolation of the log-determinant from a small fraction of the full dataset;
- we demonstrate the practical utility of our method by approximating the NTK corresponding to common deep learning models; and

Table 1: Comparison of stochastic Lanczos quadrature (SLQ, with degree l , s Monte Carlo samples, and full re-orthogonalization), MEMDET (Algorithm C.2), and FLODANCE (Algorithm 1) on a dense $500,000 \times 500,000$ NTK matrix for a ResNet50 model trained on CIFAR-10 with 50,000 datapoints. MEMDET computes the exact log-determinant and serves as the benchmark, with relative errors of other methods measured against it. Costs and wall time are based on an NVIDIA H100 GPU (\$2/hour) and an 8-core 3.6GHz CPU (\$0.2/hour) using Amazon pricing.

Method		TFLOPs	Rel. Error	Est. Cost	Wall Time
Name	Settings				
SLQ	$l = 100, s = 104$	5203	55%	\$83	1.8 days
MEMDET	LDL, $n_b = 32$	41,667	0%	\$364	8.8 days
FLODANCE	$n_s = 500, q = 0$	0.04	4%	\$0.04	1 min
FLODANCE	$n_s = 5000, q = 4$	41.7	0.02%	\$4	1.5 hr

- we provide a high-performance Python package `detkit`¹, which implements the presented algorithms and can be used to reproduce the results of this paper.

Crucially, we demonstrate that our approximation technique is able to obtain estimates with lower error than incurred by reducing the numerical precision used in explicit computation. Our approximation techniques render an impractical task *virtually routine*, as shown in Table 1. To the best of our knowledge, this is the first time that the full empirical NTK corresponding to a dataset of this scale has been computed.

The remainder of this document is structured as follows. In Section 2, we discuss the computational issues faced when computing determinants at scale, and we derive our MEMDET algorithm based on block LU computation of the log-determinant. Section 3 contains the appropriate scaling laws for pseudo-determinants of interest, the corresponding LLN and CLT for their logarithms, and the FLODANCE algorithm for their approximation. Numerical experiments are presented in Section 4, and we conclude in Section 5.

2 Computing Determinants at Scale

The computation of determinants of large matrices, particularly those expected to be highly ill-conditioned, is widely considered to be a computationally “ugly” problem, which should be avoided, if possible (Axler, 1995). However, this is not always an option, for example when the determinant represents a volume form, is required in a determinantal point process, or plays a role in training GPs via empirical Bayes. Although certain limiting behaviors under expectation are well characterized (Hodgkinson et al., 2023a), they provide only a coarse approximation in finite-sample settings. The quadratic memory cost and cubic computational complexity of naïve implementations make exact computation prohibitive, necessitating the use of lower-precision or randomized methods at scale. While approximate methods can be useful in their own right, exact computation remains essential, at the very least, to establish meaningful baselines. In our experiments, due to the pathological spectral behavior of the matrices we consider, we will see that our proposed exact method is comparable in speed to the state-of-the-art Monte Carlo approximation techniques.

2.1 Low-Precision Arithmetic

Among the most common techniques for circumventing memory and computational bottlenecks when dealing with large-scale calculations in numerical linear algebra is to cast numerical values into a lower precision, usually 32-bit, 16-bit, or even 8-bit floating point values, instead of 64-bit (double precision) values that would otherwise be used.

Computations of the log-determinant in mixed precision do not generally incur significant error. However, in our setting, the matrix of interest is realized as the product $\mathbf{J}\mathbf{J}^\top$, where \mathbf{J} is the Jacobian. The formation of

¹For details see Appendix I.

the quadratic is a well-known source of approximation error, and should be avoided if possible: paraphrasing Higham (2022), if δ is the round-off used in choice of floating point arithmetic, then for $0 < \varepsilon < \sqrt{\delta}$ we can consider the simple case of $\mathbf{J} = \begin{bmatrix} 1 & \varepsilon \\ 1 & 0 \end{bmatrix}$, we have

$$\mathbf{J}\mathbf{J}^\top = \begin{bmatrix} 1 + \varepsilon^2 & 1 \\ 1 & 1 \end{bmatrix}, \quad \text{fl}(\mathbf{J}\mathbf{J}^\top) = \begin{bmatrix} 1 & 1 \\ 1 & 1 \end{bmatrix},$$

where $\mathbf{J}\mathbf{J}^\top$ rounds to the singular $\text{fl}(\mathbf{J}\mathbf{J}^\top)$. In general, significant precision loss should occur if $\text{cond}(\mathbf{J}\mathbf{J}^\top) > \delta^{-1}$, where $\delta \approx 10^{-3}$, 10^{-6} , and 10^{-15} for 16-bit, 32-bit, and 64-bit precisions respectively. In the Gram matrices we consider, $\text{cond}(\mathbf{J}\mathbf{J}^\top) > 10^{12}$. Due to the scale of the problems of interest here, the sheer size of the Jacobian (requiring at least hundreds of terabytes of space) makes directly operating on \mathbf{J} impractical. This necessitates breaking conventional wisdom and explicitly forming the Gram matrix. We will see later the incurred cost to accuracy when working in low precision.

2.2 MEMDET: A Memory-Constrained Algorithm for Log-Determinant Computation

Conventional methods for computing the determinant of matrices include LU decomposition (for generic matrices), LDL decomposition (for symmetric matrices), and Cholesky decomposition (for symmetric positive-definite matrices). These methods also simultaneously provide the determinants of all sub-matrices $\mathbf{M}_{[k,:;k]}$, consisting of the first k rows and columns ($k = 1, \dots, m$) of the $m \times m$ matrix \mathbf{M} . This will be beneficial in our applications.

The LU decomposition has a computational complexity of approximately $\frac{2}{3}m^3$, while both LDL and Cholesky decompositions have a complexity of approximately $\frac{1}{3}m^3$. While computational complexity is a primary concern for large-scale determinant computation, memory limitation poses an even greater challenge. These methods require substantial memory allocation, either the size of the array if written in-place, or twice the size if the input array is preserved.

To address this, we present MEMDET, a memory-constrained algorithm for large-scale determinant computation. Below is a sketch of the algorithm, with details of its implementation, memory and computational aspects provided in Appendix C, and a description of the software implementing this algorithm provided in Appendix I. We focus on the algorithm for generic matrices using LU decomposition, though the LDL and Cholesky decompositions follow similarly.

Consider the 2×2 block LU decomposition of \mathbf{M} (see for instance Dongarra et al. (1998b, Chapter 5.4)) with the first block, \mathbf{M}_{11} , of size $b \times b$, $b < m$, as

$$\mathbf{M} = \begin{bmatrix} \mathbf{M}_{11} & \mathbf{M}_{12} \\ \mathbf{M}_{21} & \mathbf{M}_{22} \end{bmatrix} = \begin{bmatrix} \mathbf{L}_{11} & \mathbf{0} \\ \mathbf{L}_{21} & \mathbf{I} \end{bmatrix} \begin{bmatrix} \mathbf{U}_{11} & \mathbf{U}_{12} \\ \mathbf{0} & \mathbf{S} \end{bmatrix}, \quad (1)$$

where \mathbf{L}_{11} is lower triangular, \mathbf{U}_{11} is upper-triangular, and \mathbf{I} is the identity matrix. The blocks of the decomposition are obtained by computing $\mathbf{M}_{11} = \mathbf{L}_{11}\mathbf{U}_{11}$, solving lower-triangular system $\mathbf{U}_{12} = \mathbf{L}_{11}^{-1}\mathbf{M}_{12}$ and upper-triangular system $\mathbf{L}_{21} = \mathbf{M}_{21}\mathbf{U}_{11}^{-1}$, and forming the Schur complement $\mathbf{S} := \mathbf{M}_{22} - \mathbf{L}_{21}\mathbf{U}_{12}$. This procedure is then repeated on the $(m - b) \times (m - b)$ matrix \mathbf{S} , treated as the new \mathbf{M} , leading to a new $b \times b$ upper-triangular matrix \mathbf{U}_{11} and a smaller Schur complement \mathbf{S} at each iteration. This hierarchical procedure continues until the remaining \mathbf{S} is of size b or less, at which point its LU decomposition is computed. The log-determinant of the entire matrix is the sum of the log-determinants of all \mathbf{U}_{11} blocks at each iteration.

To make this memory-efficient, the algorithm is modified to hold only small chunks of the matrix in memory, storing intermediate computations on disk. Suppose \mathbf{M} consists of $n_b \times n_b$ blocks \mathbf{M}_{ij} of size $b \times b$ where $i, j = 1, \dots, n_b$. We pre-allocate four $b \times b$ matrices \mathbf{A} , \mathbf{B} , \mathbf{C} , and \mathbf{S} in memory. The k -th stage begins by loading $\mathbf{A} \leftarrow \mathbf{M}_{kk}$ from disk and performing an in-place LU decomposition $\mathbf{A} = \mathbf{L}\mathbf{U}$, with \mathbf{L} and \mathbf{U} stored in \mathbf{A} . We then compute the Schur complement for all inner blocks \mathbf{M}_{ij} , $i, j = k + 1, \dots, n_b$, by loading $\mathbf{B} \leftarrow \mathbf{M}_{kj}$ and $\mathbf{C} \leftarrow \mathbf{M}_{ik}$ from disk, solving $\mathbf{B} \leftarrow \mathbf{L}^{-1}\mathbf{B}$ and $\mathbf{C} \leftarrow \mathbf{C}\mathbf{U}^{-1}$ in-place, loading $\mathbf{S} \leftarrow \mathbf{M}_{ij}$, and computing $\mathbf{S} \leftarrow \mathbf{S} - \mathbf{C}\mathbf{B}$. The updated \mathbf{S} is then stored back to disk $\mathbf{M}_{ij} \leftarrow \mathbf{S}$, either by overwriting a block of the original matrix, or avoids this by writing to a separate scratchpad space. In the latter case, a cache

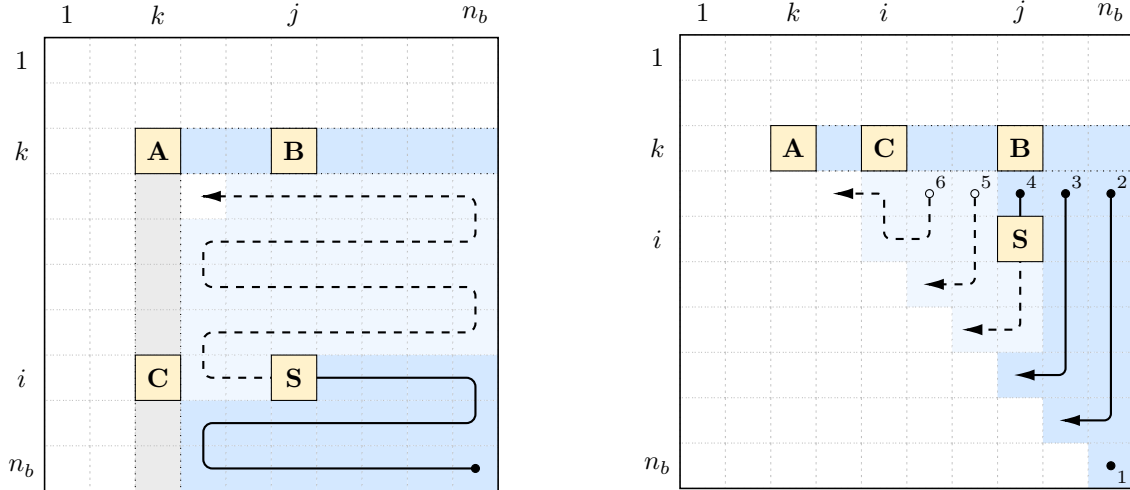


Figure 1: Schematic diagram of MEMDET illustrating the efficient block processing order for LU decomposition (Algorithm C.1, left panel) and LDL/Cholesky decompositions (Algorithm C.2, Algorithm C.3, right panel). The detailed ordering strategy is described in Appendix D.

table tracks whether a block $\mathbf{M}_{i,j}$ should be loaded from the original matrix or from the scratchpad in future calls.

The computational cost of this procedure remains the same, independent of the number of blocks, n_b (see Appendix E.1). However, increasing the number of blocks reduces memory usage at the expense of higher data transfer between disk and memory. Efficient implementation minimizes this by processing blocks in an order that reduces the loading of **B** and **C**. The left panel of Figure 1 shows one such order, illustrating the procedure at the k -th iteration. Processing the blocks $\mathbf{M}_{i,j}$ starts from the last row of the matrix and moves upward. During the horizontal and vertical traverses on the path shown in the figure, the memory blocks **C** and **B** can remain in memory, avoiding unnecessary reloading. Once the procedure reaches the block $(k+1, k+1)$, the memory block **S** can be directly read into **A** instead of being stored on disk as $\mathbf{M}_{k+1, k+1}$, initiating the block **A** for the next iteration. Consequently, only the blocks shown in blue need to be stored in the scratchpad space, while those in dark blue are already stored in the current state of the algorithm. This algorithm can be further modified to eliminate the need for **A** and use the memory space of **S** instead, but this would require storing the additional gray blocks on the scratchpad space in addition to the blue blocks. A pseudo code and further efficient implementation details of the presented method can be found as Algorithm C.1 in Appendix D.

The algorithms for LDL and Cholesky decompositions follow a similar procedure with necessary adjustments for symmetric and symmetric positive-definite matrices, as detailed in Algorithm C.2 and Algorithm C.3. These modifications include processing only the lower (or upper) triangular part of the matrix and handling permutations and diagonal scaling in the LDL decomposition. The right panel of Figure 1 shows one possible block ordering for the algorithm for LDL and Cholesky decomposition: the ordering is optimal in minimizing the number of reads and writes, but is not unique. Other block processing orderings with the same amount of data access also exist, and these will be further discussed in Appendix D. A detailed analysis of the computational complexity and memory/disk data transfers of the algorithm is provided in Appendix E. Implementation of MEMDET algorithm can be found in Listing I.1.

Although the Neural Tangent Kernel (NTK) matrices we work with are symmetric and positive definite (SPD), we do not solely rely on Cholesky decomposition, despite it being the most suitable method for SPD matrices. This is because NTK matrices can lose their positive-definiteness with even the smallest perturbations causing small eigenvalues to become negative, such as when converting from 64-bit to 32-bit precision for efficient computation. As a result, the Cholesky decomposition becomes unstable and fails, necessitating the use of LU and LDL decompositions, suitable for more general matrices. We note that the block computations of LU decomposition can become unstable as the matrices deviate from symmetric and

positive-definiteness (Demmel et al., 1995), requiring pivoting of the blocks. However, in our empirical study of NTK matrices, we found that LU decomposition works well without block pivoting, though we do consider pivoting within each block.

3 Scaling Law for the Determinant

We now turn our attention to the estimation of the log-determinant of Gram matrices corresponding to covariance kernels. Our primary motivating example is the NTK, an architecture-specific kernel associated with deep neural network models. The connections between neural networks and GP kernels are well-known, particularly the now classical results that networks at initialization induce a GP kernel in the large-width limit, enabling Bayesian inference for these infinite-width networks (Neal, 1996; Lee et al., 2018). Similarly, linearization of the gradient-flow dynamics during the late stages of training leads to the derivation of the NTK, whose infinite-width analogue can be shown to be constant during this training phase (Jacot et al., 2018; Yang, 2020; Yang & Littwin, 2021).

The NTK was first derived in the context of neural networks. However, the quantity is well defined for more a general class of functions. For a continuously differentiable function $f_\theta : \mathcal{X} \rightarrow \mathbb{R}^d$, we define its (empirical) NTK to be

$$\kappa_\theta(x, x') := \mathbf{J}_\theta(f_\theta(x))\mathbf{J}_\theta(f_\theta(x'))^\top, \quad (2)$$

where $\mathbf{J}_\theta(f_\theta(x)) \in \mathbb{R}^{d \times p}$ is the Jacobian of the function f_θ with respect to the flattened vector of its parameters $\theta \in \mathbb{R}^p$, evaluated at the point x . Note that the assumption of continuous differentiability is often relaxed in practice, and we have $\kappa_\theta(x, x') \in \mathbb{R}^{d \times d}$. When computing the NTK across n_1 and n_2 datapoints, it is typical to arrange the $n_1 n_2$ matrices as an $n_1 d \times n_2 d$ matrix. The scaling laws we derive in the sequel hold for a class of kernel functions satisfying certain decay properties on the eigenvalues of an associated integral operator (see Appendix F for a precise statement, taken from Li et al. (2023)). We remark that this class of kernels includes NTKs, as demonstrated in Bietti & Mairal (2019); Bietti & Bach (2021); Lai et al. (2023).

3.1 Neural Tangent Kernels and Scaling Laws

Let $\kappa : \mathcal{X} \times \mathcal{X} \rightarrow \mathbb{R}$ be a positive-definite kernel. For a sequence of inputs $\{x_i\}_{i=1}^\infty \subset \mathcal{X}$ and for each $n = 1, 2, \dots$, let $\mathbf{K}_n := (\kappa(x_i, x_j))_{i,j=1}^n$ be the corresponding Gram matrix for the first n inputs. Our objective is to estimate $\log \det(\mathbf{K}_n)$ for large n , using computations involving only smaller values of n . Recall that f is a Gaussian process with mean function $\mu : \mathcal{X} \rightarrow \mathbb{R}^d$ and covariance kernel $\kappa : \mathcal{X} \times \mathcal{X} \rightarrow \mathbb{R}$, denoted $f \sim \mathcal{GP}(\mu, \kappa)$, if for every $x_1, \dots, x_n \in \mathcal{X}$ and $d \geq 1$, $(f(x_i))_{i=1}^n \sim \mathcal{N}((\mu(x_i))_{i=1}^n, (\kappa(x_i, x_j))_{i,j=1}^n)$. Our results are founded on the following lemma, which we prove in Appendix G.

Lemma 1. *Let $f : \mathcal{X} \rightarrow \mathbb{R}^d$ be a zero-mean vector-valued m -dimensional Gaussian process with covariance kernel κ . For each $n \geq 2$, let*

$$E(n) := \mathbb{E}[d^{-\frac{1}{2}} \|f(x_n)\|^2 \mid f(x_i) = 0 \text{ for } i = 1, \dots, n-1],$$

denote the mean-squared error of fitting the f to the zero function using x_1, \dots, x_{n-1} . Then

$$\frac{\text{pdet}(\mathbf{K}_n)}{\text{pdet}(\mathbf{K}_{n-1})} \leq \left(\frac{d}{r}\right)^{r/2} E(n)^r,$$

where r is the rank of $\text{Cov}(f(x_n) \mid f(x_i) = 0 \text{ for } i = 1, \dots, n-1)$. In the case where $\text{rank}(\mathbf{K}_n) - \text{rank}(\mathbf{K}_{n-1}) = d$ this reduces to

$$\frac{\text{pdet}(\mathbf{K}_n)}{\text{pdet}(\mathbf{K}_{n-1})} \leq E(n)^d, \quad \text{for any } n > 1,$$

with equality if $d = 1$.

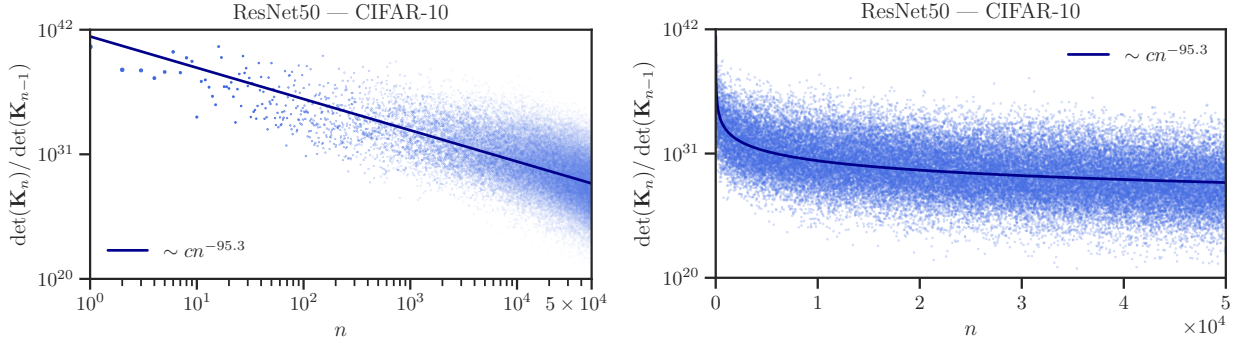


Figure 2: Demonstration of a scaling law for the ratios of successive determinants $\det(\mathbf{K}_n)/\det(\mathbf{K}_{n-1})$ (Assumption 1) for the empirical neural tangent kernel Gram matrix of a trained ResNet50 network on CIFAR-10 with $n = 50,000$ datapoints.

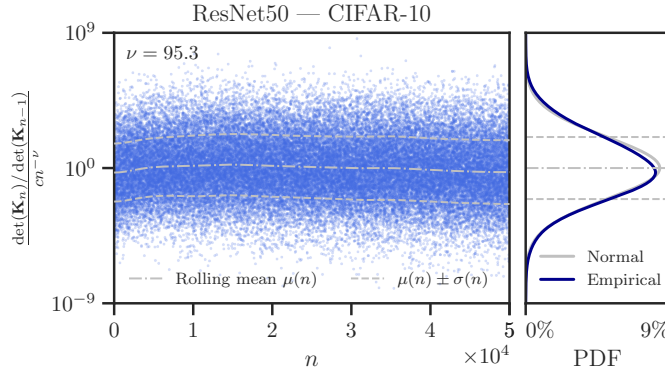


Figure 3: Demonstration of the stationarity and second moment behavior (Assumption 2) of the corresponding logarithmic process.

Lemma 1 is particularly interesting since it highlights a connection between the determinants of Gram matrices and error curves for GPs. This bounds the effect of adding or removing a datapoint on the determinant in terms of the prior variance of a corresponding GP. Previous theoretical (see [Appendix F](#)) and empirical studies ([Spigler et al., 2020](#); [Bahri et al., 2021](#); [Li et al., 2023](#); [Barzilai & Shamir, 2023](#)) have established a power law relationship of the form $E(n) = \Theta(n^{-\xi})$ as $n \rightarrow \infty$ for some $\xi > 0$. Invoking [Lemma 1](#) in view of this, we propose the following scaling law for determinants, demonstrated in [Figure 2](#).

Assumption 1 (SCALING LAW). Assume there exists a constant $C > 0$ and exponent $\nu > 0$ such that as $n \rightarrow \infty$,

$$\frac{\det(\mathbf{K}_n)}{\det(\mathbf{K}_{n-1})} = \frac{C}{n^\nu} [1 + o_p(1)]. \quad (3)$$

This assumption allows for accurate estimation of the log-determinants of interest, and an appropriate law of large numbers. However, to construct corresponding confidence intervals, we will need to assume some properties of the error term appearing in [Assumption 1](#). We further impose the mild assumptions of stationarity and bounded variance, demonstrated in [Figure 3](#).

Assumption 2 (STATIONARITY). Assume there exists a constants $C > 0$ and exponent $\nu > 0$ such that the process δ_n satisfying

$$\delta_{n-1} := \log \left(\frac{\det(\mathbf{K}_n)}{\det(\mathbf{K}_{n-1})} \right) - \log(Cn^{-\nu}), \quad n = 2, 3, \dots,$$

is stationary, ergodic, has finite second moment ($\mathbb{E}[\delta_n^2] < +\infty$), and $\mathbb{E}[\delta_n | \delta_1, \dots, \delta_{n-1}] = 0$.

Under [Assumption 1](#) and [Assumption 2](#), we derive an expression for the asymptotic behavior of the normalized log-determinants. The proof is given in [Appendix G](#).

Proposition 1. *For larger numbers of inputs, letting*

$$\begin{aligned} L_n &:= n^{-1} \log \det(\mathbf{K}_n) \\ \hat{L}_n &:= L_1 + \left(1 - \frac{1}{n}\right) c_0 - \nu \frac{\log(n!)}{n}, \end{aligned}$$

a law of large numbers (LLN) and central limit theorem (CLT) hold for the log-determinants L_n :

- (LLN) Under [Assumption 1](#), there exist constants $c_0, \nu > 0$ such that as $n \rightarrow \infty$,

$$L_n = \hat{L}_n + o_p(1). \tag{4}$$

- (CLT) Under [Assumption 2](#), there exist constants $c_0, \nu, \sigma > 0$ such that as $n \rightarrow \infty$,

$$\frac{n}{\sqrt{n-1}}(L_n - \hat{L}_n) \xrightarrow{\mathcal{D}} \mathcal{N}(0, \sigma^2). \tag{5}$$

We remark that $\log(n!)$ is $\Theta(n \log(n))$, so the normalized log-determinant L_n is $\Theta_p(\log(n))$ via (4).

3.2 FLODANCE

As (4) is linear in the unknown parameters c_0, ν , these parameters can be estimated by linear regression on a precomputed sequence² (L_1, \dots, L_n) . This sequence can be computed using a single pass of MEMDET on a subsample of the Gram matrix. After performing linear regression, by extrapolating to larger n , the normalized log-determinants of larger NTK Gram matrices can be estimated. The ordering of the data is arbitrary, but will affect the output of the regression task. We refer to this as the **F**actorial-based **L**og-**D**eterminant **A**nalysis and **N**umerical **C**urve **E**stimation procedure, or FLODANCE. To improve performance, we allow for a non-asymptotic correction to the exponent ν as $\nu(n) = \nu_0 + \sum_{i=1}^q \nu_i n^{-i}$ (in practice, we find $q = 3 \sim 6$ to work well). In light of (5) and discussion in [Appendix H](#), for large n , we expect that approximately

$$y_n = c_0 x_{n,0} + \sum_{i=1}^{q+1} \nu_{i-1} x_{n,i} + \epsilon_n, \quad \epsilon_n \sim \mathcal{N}(0, \sigma^2),$$

where $y_n = \frac{n}{\sqrt{n-1}}(L_n - L_1)$, $x_{n,0} = \sqrt{n-1}$, and $x_{n,i} = \frac{-\log(n!)}{n^{i-1}\sqrt{n-1}}$ for $i = 1, \dots, m+1$ are the covariates. The corresponding numerical procedure is presented in [Algorithm 1](#) and the implementation can be found in [Listing I.2](#).

In practice, we also observe that a burn-in period may be required to obtain accurate estimates of c_0 and the ν_i that appear in [Proposition 1](#). Better performance was often achieved in our experiments by discarding the early determinant samples, effectively replacing the L_1 term appearing in y_n with different constants L_{k+1} , for a burn-in of length k . This appears to be due to the sudden appearance of very small eigenvalues that shift the model fit, and appears to be a consistent phenomena that warrants further investigation. We found that when needed, the burn-in required was always less than 500 terms, verified by cross-validation.

4 Numerical Experiments

We are now in a position to test the accuracy of the FLODANCE algorithm for estimation of log-determinants on large-scale problems of interest. The test problems that we consider are NTK matrices corresponding to common deep learning models: ResNet9, ResNet18, and ResNet50 ([He et al., 2016](#)) trained on the CIFAR-10 dataset ([Krizhevsky, 2009](#)), and MobileNet ([Howard et al., 2017](#)) trained on the MNIST dataset ([LeCun et al., 1998](#)). Our experiments are split into two sections: first, the dataset size is reduced in order to

²This is generally a more stable regression problem than estimating C and ν directly from (3).

Algorithm 1: FLODANCE: Factorial-based Log-Determinant Analysis and Numerical Curve Estimation

Input : Precomputed partial NTK Gram matrix \mathbf{K}_{n_s} of size $m_s \times m_s$ where $m_s = n_s d$,
Number of model’s output dimension d (i.e., classes or labels)
Total number of datapoints n (i.e., training set size),
Number of datapoint samples n_s where $1 < n_s \leq n$,
Number of burn-in terms n_0 where $1 \leq n_0 < n_s$,
Number of terms in the Laurent series q

Output : Estimated normalized log-determinant \hat{L}_n of matrix \mathbf{K}_n of size $m \times m$ where $m = nd$

// Denote $\mathbf{K}_{n_s[:,k,:k]}$ the $k \times k$ principal sub-matrix of \mathbf{K}_{n_s}

- 1 Run **Algorithm C.2** on \mathbf{K}_{n_s} to obtain $(\ell_k)_{k=1}^{m_s}$ where $\ell_k \leftarrow \text{logabsdet}(\mathbf{K}_{n_s[:,k,:k]})$
- // Normalize log-determinants and record every d -th entry in the sequence.
- 2 Obtain $(L_j)_{j=n_0}^{n_s}$ where $L_j \leftarrow j^{-1} \ell_{m_j}$ and $m_j \leftarrow jd$.
- // Define design matrix $\mathbf{X} \in \mathbf{R}^{(n_s - n_0) \times (q+2)}$ and response vector $\mathbf{y} \in \mathbf{R}^{n_s - n_0}$
- 3 **for** $j = 1$ **to** $n_s - n_0$ **do**
- 4 $n_j \leftarrow n_0 + j$
- 5 $y_j \leftarrow n_j (n_j - 1)^{-\frac{1}{2}} (L_{n_j} - L_{n_0})$
- 6 $X_{j,1} \leftarrow (n_j - 1)^{\frac{1}{2}}$
- 7 **for** $i = 1$ **to** $q + 1$ **do**
- 8 $X_{j,i+1} \leftarrow -(n_j - 1)^{-\frac{1}{2}} n_j^{-i+1} \log\Gamma(n_j + 1)$ // $\log\Gamma(n + 1) = \log(n!)$ is the Log-gamma function.
- // Perform linear regression $\mathbf{y} = \mathbf{X}\beta + \epsilon$ to estimate coefficients β
- 9 $\beta \leftarrow (\mathbf{X}^\top \mathbf{X})^{-1} \mathbf{X}^\top \mathbf{y}$
- // Estimate L_n at larger value of n
- 10 $(c_0, \nu_0, \dots, \nu_q) \leftarrow \beta$
- 11 $\hat{L}_n \leftarrow L_{n_0} + c_0(1 - n^{-1}) - \sum_{i=1}^{q+1} \nu_{i-1} n^{-i} \log\Gamma(n + 1)$
- 12 **return** \hat{L}_n

Table 2: Comparison of various approximations of the normalized log-determinant \hat{L}_n with the exact computation L_n obtained in 64-bit floating-point precision (first row). Values represent averages over five trained networks, with standard deviations in parentheses. Bold values indicate the closest approximation, with the next-best underlined.

Quantity	Model	Configuration	ResNet9	ResNet9	ResNet18	MobileNet	
	Dataset		CIFAR-10	CIFAR-10	CIFAR-10	MNIST	
	Subsample Size		$n = 1000$	$n = 2500$	$n = 1000$	$n = 2500$	
L_n	Direct Computation (64-bit)	<i>(Reference)</i>	-0.490 (0.20)	-4.48 (0.26)	-15.5 (0.84)	-81.0 (3.15)	
\hat{L}_n	Direct Computation (16-bit)		9.00 (0.16)	7.89 (0.21)	-6.32 (1.07)	-26.7 (0.85)	
	Direct Computation (32-bit)		<u>2.32</u> (0.18)	<u>0.43</u> (0.22)	-12.1 (0.83)	-69.4 (2.00)	
	Block Diagonal		18.0 (0.13)	18.0 (0.17)	4.77 (1.06)	10.2 (1.40)	
	SLQ		14.2 (0.15)	13.9 (0.22)	-0.66 (1.06)	-12.5 (1.37)	
	Pseudo NTK		-13.9 (0.05)	-16.2 (0.15)	-14.89 (0.15)	-19.9 (0.19)	
	FLODANCE	$n_0 = 1, n_s = 50$		4.32 (0.46)	1.96 (0.69)	-8.40 (1.20)	-55.0 (2.20)
	FLODANCE	$n_0 = 1, n_s = 100$		3.31 (0.27)	0.91 (0.54)	-10.6 (0.70)	-54.0 (2.06)
FLODANCE	$n_0 = 300, n_s = 500$		0.53 (0.27)	-3.50 (0.33)	<u>-13.6</u> (0.43)	<u>-62.3</u> (1.13)	

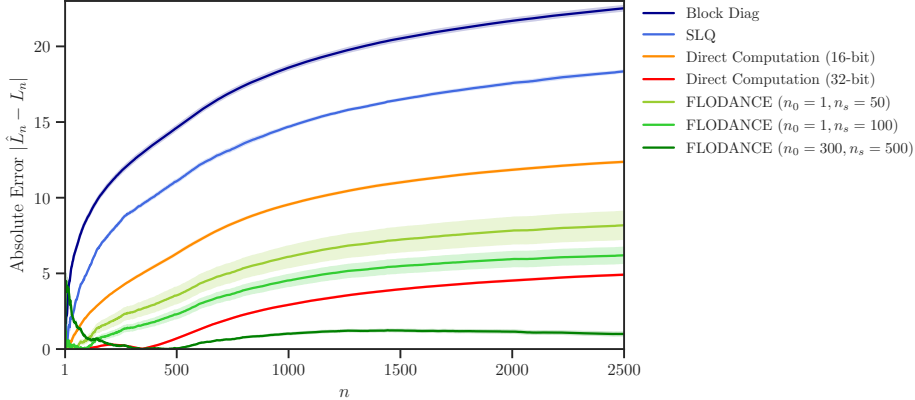


Figure 4: Comparison of log-determinant accuracy for NTKs of ResNet9 trained on CIFAR-10, measured by absolute error, across a variety of approximation techniques for matrices of different sizes. Means across five trained networks are displayed, with shaded regions depicting one standard deviation.

enable the matrices to fit into memory on a consumer device, in Section 4.1; and then larger subsamples and full datasets are considered, in Section 4.2.³ As a baseline, we employ MEMDET to compute the relevant quantities, where the accuracy is limited only by numerical precision.

4.1 Smaller Data Sets

In order to demonstrate the scaling laws for ratios of successive determinants of NTK Gram matrices, a ResNet50 model was trained on a subset of 1000 datapoints from the CIFAR-10 dataset. The resulting matrix \mathbf{K}_{1000} is of size $10,000 \times 10,000$. In Figure 2, we plot exact ratios $\det(\mathbf{K}_n)/\det(\mathbf{K}_{n-1})$, with the blue line representing the line of best fit under the scaling law Assumption 1.

For baseline comparison to existing techniques, we compared FLODANCE to approximations of both the matrices themselves and their log-determinants. For the matrix approximations, we consider a block-diagonal approximation ignoring between-data correlations, as well as the pseudo-NTK matrix studied in (Mohamadi et al., 2023). As an approximate log-determinant technique, we consider the stochastic Lanczos quadrature, often regarded as the current state-of-the-art in log-determinant estimation of large matrices (Gardner et al., 2018). We further compare the exact methods across 16-, 32- and 64-bit (treated as exact) floating-point precision, in order to compare the accuracy of our extrapolation method against memory-saving mixed-precision calculations.

To this end, ResNet9 was trained on a subsets of 1000 and 2500 images from CIFAR-10, and ResNet18 on 1000 datapoints. MobileNet was also trained on a 2500 image subset of the MNIST dataset. A comparison of the different methods is presented in Table 2. We see that all existing NTK and log-determinant approximation techniques perform poorly when compared with 16- and 32-bit mixed-precision calculations. On the other hand, the FLODANCE estimates that contained a burn-in phase consistently either outperformed the mixed-precision approximations or were competitive. When no burn-in was used, FLODANCE still outperformed the approximation methods. This suggests that at this scale, the error in the scaling law approximation is *less* than the mixed-precision errors discussed in Section 2.1. Extrapolating determinants based on expected behavior can bypass numerical issues at scale. Comparisons for ResNet9 trained on 2500 images from the CIFAR-10 dataset are visualized in Figure 4. FLODANCE estimates consistently outperform the competing methods.

³Experiments in this section were conducted on a desktop-class device with an AMD Ryzen@7 5800X processor, NVIDIA RTX 3080, and 64GB RAM.

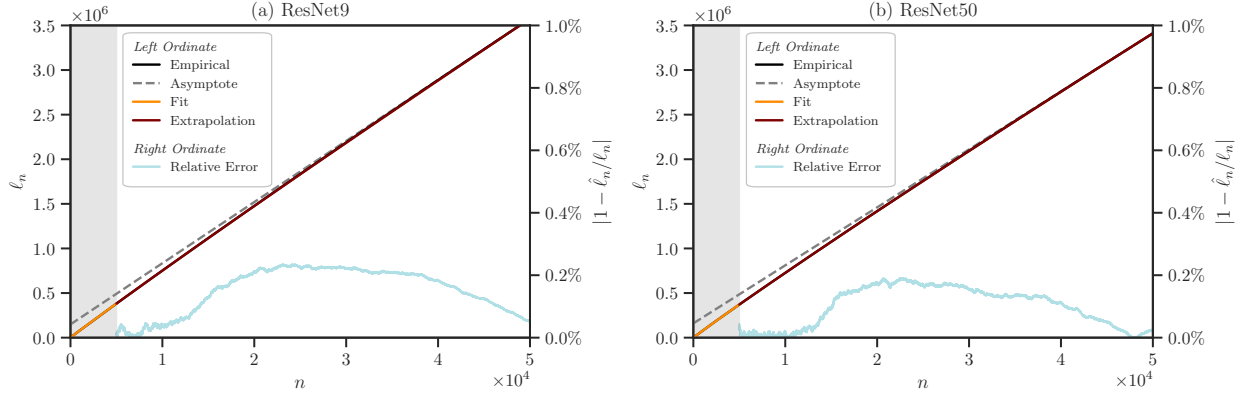


Figure 5: Log-determinant ℓ_n for $n = 1, \dots, 50,000$, corresponding to $m \times m$ NTK submatrices where $m = nd$ and $d = 10$, from ResNet9 (a) and ResNet50 (b) trained on CIFAR-10 with 50,000 datapoints. Values are computed using MEMDET (Algorithm C.2) with LDL decomposition (black curves, overlaid by colored curves). FLODANCE (Algorithm 1) is fitted in a small region (shaded gray) and extrapolated over a much larger interval. The yellow curve in the interval $(n_0, n_s) = (10^2, 5 \times 10^3)$ represents the fit, while the red curve in $(n_s, n) = (5 \times 10^3, 5 \times 10^4)$ shows the extrapolation. The blue curves, corresponding to the right axis in each panel shows the relative error, reaching impressive 0.05% in (a) and 0.02% in (b).

4.2 Larger Data Sets

In our final experiment, we evaluate NTK matrices at an unprecedented scale, where exact determinant computation has never been previously reported. Due to memory constraints, these matrices cannot be stored explicitly, making MEMDET essential for obtaining ground truth values.

We consider two large-scale NTK matrices: $\mathbf{K}_{50,000}$, a dense matrix of size $500,000 \times 500,000$, for ResNet50 trained on CIFAR-10, and an identical-sized NTK for ResNet9 trained on CIFAR-10. At this scale, double-precision arithmetic is infeasible due to memory and computational constraints, making 32-bit computation the only viable direct baseline. However, even in 32-bit, these matrices require nearly a terabyte of storage.

As shown in Figure 5, FLODANCE with $q = 6$, $n_0 = 100$, and $n_s = 5000$ achieves an absolute error of just 0.05% for $L_{50,000}$ on ResNet9, reducing computation time by a factor of $(n/n_s)^3 = 1000$. Similarly, for ResNet50, FLODANCE with $q = 4$, $n_0 = 100$, and $n_s = 5000$ achieves an absolute error of 0.02% with the same speedup. In contrast, SLQ exhibited a relative error of 55% (see Table 1, also Listing I.3 for implementation). Given their poor performance on smaller datasets, pseudo-NTK and block-diagonal approximations are omitted.

This experiment represents the first exact computation of an NTK determinant at this scale, establishing a new benchmark for large-scale log-determinant estimation.

5 Conclusion

The calculation of large matrix log-determinants is a commonly encountered but often avoided problem when considering statistical and machine learning problems at scale. A number of techniques have previously been proposed to circumvent explicit computation, typically relying upon stochastic approximations. However, in many problems of interest the sheer size of the matrices, combined with their highly ill-conditioned nature, make not only approximation a difficult task, but forming the matrix itself to provide a baseline becomes computationally intractable. We have addressed this problem on two fronts. On the one hand, we defined MEMDET, a hierarchical memory-constrained algorithm for log-determinant computation, with different versions for general, symmetric, and symmetric positive-definite matrices. On the other hand, we derived neural scaling laws for large kernel matrices, and introduced FLODANCE, a procedure for accurate extrapolation of log-determinants from small subsets of the data. The high level of speed and accuracy of our methods opens the door for routine computation of the interpolating information criteria and related

diagnostic tools to enable principled model selection within deep learning frameworks (Hodgkinson et al., 2023b).

The ability to accurately compute and estimate matrices of this size further provides fascinating insights into the behavior of the NTKs that we considered in our experiments, which considered square matrices of the size up to 500,000. Further, the memory constrained algorithms we considered can be applied to other classes of matrices (Nguyen & Vu, 2014; Cai et al., 2015), where they can be expected to unlock similar insights into their scaling behavior. In terms of further computational tools, we hope for the development of blockwise decompositions of large scale Jacobian matrices, in order to circumvent the need to explicitly calculate $\mathbf{J}\mathbf{J}^\top$.

Acknowledgments. LH is supported by the Australian Research Council through a Discovery Early Career Researcher Award (DE240100144). FR was partially supported by the Australian Research Council through an Industrial Transformation Training Centre for Information Resilience (IC200100022). MWM would like to acknowledge the DOE, IARPA, NSF, and ONR for providing partial support of this work.

References

- Ameli, S. & Shadden, S. C. (2023). A singular Woodbury and pseudo-determinant matrix identities and application to Gaussian process regression. *Applied Mathematics and Computation*, 452, 128032.
- Axler, S. (1995). Down with determinants! *The American Mathematical Monthly*, 102.
- Bahri, Y., Dyer, E., Kaplan, J., Lee, J., & Sharma, U. (2021). Explaining neural scaling laws. *arXiv preprint arXiv:2102.06701*.
- Barrachina, S., Castillo, M., Igual, F. D., Mayo, R., & Quintana-Ortí, E. S. (2008). Solving dense linear systems on graphics processors. In *Euro-Par 2008 – Parallel Processing* (pp. 739–748). Berlin, Heidelberg: Springer Berlin Heidelberg.
- Barzilai, D. & Shamir, O. (2023). Generalization in kernel regression under realistic assumptions. *arXiv preprint arXiv:2312.15995*.
- Bietti, A. & Bach, F. (2021). Deep equals shallow for ReLU networks in kernel regimes. In *International Conference on Learning Representations*.
- Bietti, A. & Mairal, J. (2019). On the inductive bias of neural tangent kernels. In H. Wallach, H. Larochelle, A. Beygelzimer, F. d'Alché-Buc, E. Fox, & R. Garnett (Eds.), *Advances in Neural Information Processing Systems*, volume 32: Curran Associates, Inc.
- Billingsley, P. (1961). The Lindeberg-Levy theorem for martingales. *Proceedings of the American Mathematical Society*, 12(5), 788–792.
- Cai, T. T., Liang, T., & Zhou, H. H. (2015). Law of log determinant of sample covariance matrix and optimal estimation of differential entropy for high-dimensional Gaussian distributions. *Journal of Multivariate Analysis*, 137, 161–172.
- Chizat, L., Oyallon, E., & Bach, F. (2019). On lazy training in differentiable programming. In H. Wallach, H. Larochelle, A. Beygelzimer, F. d'Alché-Buc, E. Fox, & R. Garnett (Eds.), *Advances in Neural Information Processing Systems*, volume 32: Curran Associates, Inc.
- Demmel, J. W., Heath, M. T., & van der Vorst, H. A. (1993). Parallel numerical linear algebra. *Acta Numerica*, 2, 111–197.
- Demmel, J. W., Higham, N. J., & Schreiber, R. S. (1995). Stability of block LU factorization. *Numerical Linear Algebra with Applications*, 2(2), 173–190.
- Dong, K., Eriksson, D., Nickisch, H., Bindel, D., & Wilson, A. G. (2017). Scalable log determinants for Gaussian process kernel learning. In I. Guyon, U. V. Luxburg, S. Bengio, H. Wallach, R. Fergus, S.

- Vishwanathan, & R. Garnett (Eds.), *Advances in Neural Information Processing Systems*, volume 30: Curran Associates, Inc.
- Dongarra, J., Hammarling, S., & Walker, D. (1998a). Key concepts for parallel out-of-core LU factorization. *Computers & Mathematics with Applications*, 35(7), 13–31. Advanced Computing on Intel Architectures.
- Dongarra, J. J., Duff, L. S., Sorensen, D. C., & Vorst, H. A. V. (1998b). *Numerical Linear Algebra for High Performance Computers*. USA: Society for Industrial and Applied Mathematics.
- Dongarra, J. J., Moler, C. B., Bunch, J. R., & Stewart, G. W. (1979). *LINPACK Users' Guide*. Society for Industrial and Applied Mathematics.
- Engel, A., Wang, Z., Sarwate, A. D., Choudhury, S., & Chiang, T. (2022). TorchNTK: A Library for Calculation of Neural Tangent Kernels of PyTorch Models.
- Fischer, S. & Steinwart, I. (2020). Sobolev norm learning rates for regularized least-squares algorithms. *Journal of Machine Learning Research*, 21(205), 1–38.
- Fitzsimons, J., Cutajar, K., Osborne, M., Roberts, S., & Filippone, M. (2017). Bayesian Inference of Log Determinants. In *Proceedings of the 33rd Conference on Uncertainty in Artificial Intelligence*, Proceedings of Machine Learning Research Sydney, Australia: PMLR.
- Galoppo, N., Govindaraju, N., Henson, M., & Manocha, D. (2005). LU-GPU: Efficient algorithms for solving dense linear systems on graphics hardware. In *SC '05: Proceedings of the 2005 ACM/IEEE Conference on Supercomputing* (pp. 3–3).
- Gardner, J., Pleiss, G., Weinberger, K. Q., Bindel, D., & Wilson, A. G. (2018). GPyTorch: Blackbox matrix-matrix Gaussian process inference with GPU acceleration. *Advances in neural information processing systems*, 31.
- Gelman, A., Carlin, J. B., Stern, Dunson, D. B., Vehtari, A., & Rubin, D. B. (2013). *Bayesian Data Analysis*. Chapman and Hall/CRC, 3rd ed. edition.
- Gholami, A., Yao, Z., Kim, S., Hooper, C., Mahoney, M. W., & Keutzer, K. (2024). AI and memory wall. *IEEE Micro*.
- Golub, G. H. & Van Loan, C. F. (2013). *Matrix Computations - 4th Edition*. Philadelphia, PA: Johns Hopkins University Press.
- He, K., Zhang, X., Ren, S., & Sun, J. (2016). Deep residual learning for image recognition. In *Proceedings of the IEEE conference on computer vision and pattern recognition* (pp. 770–778).
- Higham, N. (2022). Seven Sins of Numerical Linear Algebra. <https://nhigham.com/2022/10/11/seven-sins-of-numerical-linear-algebra/>. Accessed: 2024-05-21.
- Hodgkinson, L., Van Der Heide, C., Roosta, F., & Mahoney, M. W. (2023a). Monotonicity and double descent in uncertainty estimation with Gaussian processes. In *Proceedings of the 40th International Conference on Machine Learning* (pp. 13085–13117).
- Hodgkinson, L., van der Heide, C., Salomone, R., Roosta, F., & Mahoney, M. W. (2023b). The interpolating information criterion for overparameterized models. *arXiv preprint arXiv:2307.07785v1*.
- Hodgkinson, L., van der Heide, C., Salomone, R., Roosta, F., & Mahoney, M. W. (2023c). A PAC-Bayesian perspective on the interpolating information criterion. In *Advances in Neural Information Processing Systems*, Mathematics of Modern Machine Learning Workshop.
- Hoffmann, J., Borgeaud, S., Mensch, A., Buchatskaya, E., Cai, T., Rutherford, E., de Las Casas, D., Hendricks, L. A., Welbl, J., Clark, A., Hennigan, T., Noland, E., Millican, K., van den Driessche, G., Damoc, B., Guy, A., Osindero, S., Simonyan, K., Elsen, E., Vinyals, O., Rae, J., & Sifre, L. (2022). An empirical analysis of compute-optimal large language model training. In S. Koyejo, S. Mohamed, A. Agarwal, D. Belgrave, K. Cho, & A. Oh (Eds.), *Advances in Neural Information Processing Systems*,

- volume 35 (pp. 30016–30030): Curran Associates, Inc.
- Howard, A. G., Zhu, M., Chen, B., Kalenichenko, D., Wang, W., Weyand, T., Andreetto, M., & Adam, H. (2017). Mobilenets: Efficient convolutional neural networks for mobile vision applications. *arXiv preprint arXiv:1704.04861*.
- Immer, A., Korzepa, M., & Bauer, M. (2021). Improving predictions of bayesian neural nets via local linearization. In A. Banerjee & K. Fukumizu (Eds.), *Proceedings of The 24th International Conference on Artificial Intelligence and Statistics*, volume 130 of *Proceedings of Machine Learning Research* (pp. 703–711): PMLR.
- Immer, A., Van Der Ouderaa, T. F. A., Van Der Wilk, M., Ratsch, G., & Schölkopf, B. (2023). Stochastic marginal likelihood gradients using neural tangent kernels. In A. Krause, E. Brunskill, K. Cho, B. Engelhardt, S. Sabato, & J. Scarlett (Eds.), *Proceedings of the 40th International Conference on Machine Learning*, volume 202 of *Proceedings of Machine Learning Research* (pp. 14333–14352): PMLR.
- Jacot, A., Gabriel, F., & Hongler, C. (2018). Neural tangent kernel: Convergence and generalization in neural networks. In S. Bengio, H. Wallach, H. Larochelle, K. Grauman, N. Cesa-Bianchi, & R. Garnett (Eds.), *Advances in Neural Information Processing Systems*, volume 31: Curran Associates, Inc.
- Kaplan, J., McCandlish, S., Henighan, T., Brown, T. B., Chess, B., Child, R., Gray, S., Radford, A., Wu, J., & Amodei, D. (2020). Scaling laws for neural language models. *arXiv preprint arXiv:2001.08361*.
- Karlin, S. & McGregor, J. (1959). Coincidence probabilities. *Pacific Journal of Mathematics*, 9(4), 1141 – 1164.
- Kim, S., Park, S., Kim, K.-S., & Yang, E. (2023). Scale-invariant Bayesian neural networks with connectivity tangent kernel. In *The Eleventh International Conference on Learning Representations*.
- Krizhevsky, A. (2009). *Learning multiple layers of features from tiny images*. Technical Report TR-2009, University of Toronto.
- Kulesza, A., Taskar, B., et al. (2012). Determinantal point processes for machine learning. *Foundations and Trends® in Machine Learning*, 5(2–3), 123–286.
- Lai, J., Xu, M., Chen, R., & Lin, Q. (2023). Generalization ability of wide neural networks on \mathbb{R} .
- LeCun, Y., Bottou, L., Bengio, Y., & Haffner, P. (1998). Gradient-based learning applied to document recognition. *Proceedings of the IEEE*, 86(11), 2278–2324.
- Lee, J., Sohl-dickstein, J., Pennington, J., Novak, R., Schoenholz, S., & Bahri, Y. (2018). Deep neural networks as Gaussian processes. In *International Conference on Learning Representations*.
- Li, Y., Zhang, H., & Lin, Q. (2023). On the asymptotic learning curves of kernel ridge regression under power-law decay. In A. Oh, T. Naumann, A. Globerson, K. Saenko, M. Hardt, & S. Levine (Eds.), *Advances in Neural Information Processing Systems*, volume 36 (pp. 49341–49364): Curran Associates, Inc.
- Mézard, M. & Montanari, A. (2009). *Information, Physics, and Computation*. Oxford University Press.
- Mohamadi, M. A., Bae, W., & Sutherland, D. J. (2023). A fast, well-founded approximation to the empirical neural tangent kernel. In A. Krause, E. Brunskill, K. Cho, B. Engelhardt, S. Sabato, & J. Scarlett (Eds.), *Proceedings of the 40th International Conference on Machine Learning*, volume 202 of *Proceedings of Machine Learning Research* (pp. 25061–25081): PMLR.
- Neal, R. M. (1996). *Bayesian Learning for Neural Networks*. Berlin, Heidelberg: Springer-Verlag.
- Nguyen, H. H. & Vu, V. (2014). Random matrices: Law of the determinant. *The Annals of Probability*, 42(1), 146 – 167.
- Novak, R., Sohl-Dickstein, J., & Schoenholz, S. S. (2022). Fast finite width neural tangent kernel. In

- International Conference on Machine Learning* (pp. 17018–17044).: PMLR.
- Rasmussen, C. E. & Williams, C. K. I. (2006). *Gaussian Processes for Machine Learning*. MIT Press Cambridge.
- Rue, H. & Held, L. (2005). *Gaussian Markov Random Fields: Theory and Applications*. Chapman and Hall/CRC.
- Smith, T. (2023). An exabyte of disk storage at CERN. <https://home.cern/news/news/computing/exabyte-disk-storage-cern>. Accessed: 2024-07-18.
- Spigler, S., Geiger, M., & Wyart, M. (2020). Asymptotic learning curves of kernel methods: empirical data versus teacher–student paradigm. *Journal of Statistical Mechanics: Theory and Experiment*, 2020(12), 124001.
- Stark, S. & Beris, A. N. (1992). LU decomposition optimized for a parallel computer with a hierarchical distributed memory. *Parallel Computing*, 18(9), 959–971.
- Steinwart, I., Hush, D. R., & Scovel, C. (2009). Optimal rates for regularized least squares regression. In *COLT*.
- Ubaru, S., Chen, J., & Saad, Y. (2017). Fast Estimation of $\text{tr}(f(A))$ via Stochastic Lanczos Quadrature. *SIAM Journal on Matrix Analysis and Applications*, 38(4), 1075–1099.
- Vakili, S., Bromberg, M., Garcia, J. R., shan Shiu, D., & Bernacchia, A. (2022). Uniform generalization bounds for overparameterized neural networks.
- Venetis, I. E. & Gao, G. R. (2009). Mapping the LU decomposition on a many-core architecture: challenges and solutions. In *Proceedings of the 6th ACM Conference on Computing Frontiers, CF '09* (pp. 71–80). New York, NY, USA: Association for Computing Machinery.
- Wang, K., Pleiss, G., Gardner, J., Tyree, S., Weinberger, K. Q., & Wilson, A. G. (2019). Exact Gaussian processes on a million data points. *Advances in neural information processing systems*, 32.
- Yang, G. (2020). Tensor programs II: Neural tangent kernel for any architecture. *ArXiv*, abs/2006.14548.
- Yang, G. & Littwin, E. (2021). Tensor programs IIb: Architectural universality of neural tangent kernel training dynamics. In M. Meila & T. Zhang (Eds.), *Proceedings of the 38th International Conference on Machine Learning*, volume 139 of *Proceedings of Machine Learning Research* (pp. 11762–11772).: PMLR.

Appendices

Contents

A Related Works	16
B Memory and Computation Challenges of NTK Matrices	17
C Implementation of MEMDET Algorithm	18
D Optimal Sequence of Processing of Blocks	18
E Complexity and Performance Analysis of MEMDET	22
E.1 Computational Complexity	22
E.2 Data Transfer and Memory Considerations	23
E.3 Empirical Performance Evaluation	24
E.4 Concluding Remarks of Performance Analysis	25
F Background Material for Neural Scaling Laws	26
G Proofs of Lemma 1 and Proposition 1	27
H Derivation of FLODANCE Parameterization	28
I Implementation and Reproducibility Guide	29

Appendix A Related Works

The study of block decomposition methods in numerical linear algebra has a long history. Classical texts such as [Golub & Van Loan \(2013\)](#) and [Dongarra et al. \(1998b\)](#) provide foundational discussions on block LU, block Cholesky, and LDL decompositions, detailing their computational advantages and numerical properties. These methods have been widely used to improve computational efficiency, particularly in high-performance computing (HPC) settings, where recursive block LU ([Golub & Van Loan, 2013, Section 3.2.11](#)), parallel LU ([Golub & Van Loan, 2013, Section 3.6](#)), and block Cholesky ([Golub & Van Loan, 2013, Section 4.2.9](#)) play a central role in large-scale matrix computations.

Beyond theoretical foundations, numerous works have focused on efficient implementations of block factorizations, particularly for parallel architectures. [Stark & Beris \(1992\)](#) optimized block LU decomposition for hierarchical distributed memory, aiming to improve data locality while maintaining parallel efficiency. [Dongarra et al. \(1979\)](#) pioneered high-performance implementations of block factorizations, laying the groundwork for modern HPC systems. More recent studies, such as [Galoppo et al. \(2005\)](#) and [Barrachina et al. \(2008\)](#), have extended block LU methods to GPU-based environments, leveraging parallelism but still assuming that intermediate submatrices fit in memory. While these approaches optimize performance in parallel settings, they do not address the challenge of computing factorizations when the full matrix size far exceeds available RAM. Traditional block methods typically assume that at least some intermediate submatrices can reside in memory, whereas our method (MEMDET) explicitly operates under constrained memory settings, utilizing an out-of-core hierarchical block processing approach.

To address the issue of matrices exceeding main memory capacity, [Dongarra et al. \(1998a\)](#) introduced concepts for parallel out-of-core LU factorization, focusing on efficient data movement between disk and memory. While their work demonstrates how out-of-core computations can be applied to LU factorization, their approach does not extend to log-determinant computations or hierarchical block-wise processing. Similarly, studies on many-core architectures ([Venetis & Gao, 2009](#)) and hierarchical memory-aware LU factorizations ([Demmel et al., 1993](#)) have improved computational efficiency, but none have been designed specifically for computing log-determinants under extreme memory constraints, making our approach distinct.

Table B.1: Memory requirements (for different data type precisions) to store empirical NTK matrices of common datasets.

Dataset	Training Set	Classes	Matrix Size		
			float16	float32	float64
CIFAR-10	50,000	10	0.5 TB	1.0 TB	2.0 TB
MNIST	60,000	10	0.72 TB	1.5 TB	2.9 TB
SVHN	73,257	10	1.1 TB	2.2 TB	4.2 TB
ImageNet-1k	1,281,167	1000	3,282,778 TB	6,565,556 TB	13,131,111 TB

Table B.2: Estimated compute time (in hours using NVIDIA H100 GPU) for NTK matrix computation.

Dataset	Model	Compute Time (hrs)		
		float16	float32	float64
MNIST	MobileNet	6	25	50
CIFAR-10	ResNet9	6	24	70
	ResNet18	14	63	65
	ResNet50	37	177	297
	ResNet101	107	442	1178

Appendix B Memory and Computation Challenges of NTK Matrices

The empirical NTK serves as a motivating example throughout this work, as it encapsulates many of the computational challenges associated with large-scale matrix operations. Several software packages have been developed to compute NTK Gram matrices for different neural architectures using automatic differentiation frameworks (Novak et al., 2022; Engel et al., 2022). However, the full formation of these matrices remains computationally prohibitive, even on commonly used benchmark datasets.

Table B.1 presents the storage requirements for NTK matrices corresponding to various datasets, highlighting their enormous size. For instance, even CIFAR-10 requires terabytes of storage, while ImageNet-1k exceeds *exabytes*, making full NTK computation infeasible for most practical applications. Despite its theoretical importance, the NTK Gram matrix is rarely used as a practical tool, with approximations often employed to mitigate computational and memory constraints. Minibatching is one common strategy, and batch-wise NTK approximations have been explored for model selection (Immer et al., 2023), yet extending these estimates to full datasets remains an open challenge. Alternative approximation techniques (Mohamadi et al., 2023) have been proposed, but their convergence is only guaranteed in spectral norm, limiting their ability to capture the full spectrum of the NTK. In contrast, the log-determinant—a key quantity in this work—encodes information from the entire eigenvalue distribution, making its computation particularly demanding.

Beyond storage limitations, the computation time for NTK matrices also presents a major challenge. Table B.2 provides estimated compute times for NTK formation across various models and floating-point precisions on an NVIDIA H100 GPU. Even for relatively small datasets like CIFAR-10, NTK computation is expensive, with higher-precision calculations significantly increasing runtime. For large architectures such as ResNet101, double-precision NTK computation can require over a thousand hours, making exact evaluations impractical without algorithmic improvements like those introduced in this work.

Appendix C Implementation of MEMDET Algorithm

The pseudo-code of MEMDET algorithm is given in [Algorithm C.1](#) (for generic matrices), [Algorithm C.2](#) (for symmetric matrices), and [Algorithm C.3](#) (for symmetric positive-definite matrices), which computes the log-determinant of the matrix \mathbf{M} . We note that the log-determinant of all sub-matrices $\mathbf{M}_{[k:k, k]}$, or their row/column permutations for $k = 1, \dots, m$, can also be readily computed. For instance, for symmetric and positive-definite matrices using Cholesky decomposition $\mathbf{M} = \mathbf{L}\mathbf{L}^\top$, with lower-triangular matrix \mathbf{L} , the logarithm of its positive determinant is $\log\det(\mathbf{M}_{[k:k, k]}) = 2 \sum_{i=1}^k \log(L_{ii})$.

The memory requirements of MEMDET are determined by a user-defined parameter, allowing it to run on any system regardless of available memory. For an $m \times m$ matrix, the algorithm partitions the data into an $n_b \times n_b$ grid of blocks, each of size $b \times b$, where $b = 1 + \lfloor (m-1)/n_b \rfloor$. The computation requires either 3 or 4 concurrent blocks in memory: for $n_b = 2$, only 3 blocks are needed, requiring $3b^2\beta$ bytes, while for $n_b > 2$, 4 blocks are required, increasing the memory usage to $4b^2\beta$ bytes, where β is the number of bytes per floating point.

Given a maximum memory limit c (in bytes), the optimal number of blocks n_b is determined by the parameter $r = m\sqrt{\beta}/c$, with the following selection criteria:

- If $r \leq 1$, the entire matrix fits in memory, so $n_b = 1$.
- If $r \leq \frac{2}{\sqrt{3}}$, three blocks fit in memory, so $n_b = 2$.
- Otherwise, $n_b = \lceil 2r \rceil$.

Appendix D Optimal Sequence of Processing of Blocks

It is important to select an ordering of the blocks to minimize data transfer between disk and memory. The order in which the block \mathbf{M}_{ij} is processed should be chosen to minimize the reading of the blocks \mathbf{B} (corresponding to the index j) and \mathbf{C} (corresponding to the index i). Ideally, from processing one block to the next, one should update only one of the matrices \mathbf{B} or \mathbf{C} , but not both, to reuse one of the blocks already loaded in memory. We formulate this problem of finding the optimal sequence of blocks as follows for the case of LDL/Cholesky decomposition at the k -th stage of the algorithm. The case for LU decomposition can be formulated similarly.

Let $G(V, E)$ denote a complete undirected graph with vertices $V := \{k+1, \dots, n_b\}$, where E is the set of all possible edges $e = (v, u)$ between the vertices $u, v \in V$. Each vertex in V represents the event of loading one of the blocks $\mathbf{B} \leftarrow \mathbf{M}_{kj}$ or $\mathbf{C} \leftarrow \mathbf{M}_{ik}$, $i, j = k+1, \dots, n_b$. Each edge in E corresponds to the event of processing the block \mathbf{M}_{ij} . At the k -th stage of the algorithm, eventually, all blocks $i, j = k+1, \dots, n_b$ will be processed, so E consists of all edges of a complete graph, including self-loops, with $|E| = \frac{|V|(|V|+1)}{2}$. To illustrate this concept, consider the example in [Figure D.1](#). The left panel depicts the k -th iteration of the algorithm for a symmetric matrix, where the matrices \mathbf{B} and \mathbf{C} have four blocks to choose from the set $V = \{v_1, v_2, v_3, v_4\}$. The corresponding graph G is shown in the middle panel of the figure.

The goal is to select an ordered sequence (e_p) , $p = 1, \dots, |E|$ of edges such that each two consecutive edges e_p and e_{p+1} in the sequence share a common vertex. This ensures that from processing one block to the next, only one of \mathbf{B} or \mathbf{C} is updated, while at least one block is reused from the previous step.

To find such a sequence of edges, we define $L(G)$, the *line graph* of G (also known as the *edge-to-vertex dual*), where each vertex of $L(G)$ represents an edge of G . Two vertices in $L(G)$ are connected if and only if their corresponding edges in G share a common vertex. Consequently, any *Hamiltonian path* in $L(G)$ defines an ordered sequence of edges that fulfills our requirement.

As illustrated in [Figure D.1](#), the right panel depicts the line graph of the given graph shown in the middle panel, with a possible Hamiltonian path highlighted in red. This path directly translates to the processing order of blocks shown in the left panel. Notably, all valid Hamiltonian paths must terminate at the node e_1 , representing the block $\mathbf{M}_{k+1, k+1}$. This specific end point is crucial as it allows for a seamless transition to the next iteration (i.e., the $k+1$ iteration) without the need to explicitly load the matrix \mathbf{A} , as it would already be available in memory from the last processing block of the k -th iteration when $\mathbf{S} \leftarrow \mathbf{M}_{k+1, k+1}$ was processed.

Algorithm C.1: MEMDET: Constrained-Memory Comp. of Log-Det (Case I: *Generic Matrix*)

Input : Matrix \mathbf{M} of size $m \times m$, *// stored on disk, may not be loaded on memory*
Maximum memory c in bytes

Output : ℓ : logarithm of the absolute value of the determinant (`logabsdet`) of \mathbf{M} ,
 σ : sign of the determinant of \mathbf{M}

```

1  $r \leftarrow m\sqrt{\beta/c}$  //  $\beta$ : number of bytes per floating-point
2 if  $r \leq 1$  then  $n_b \leftarrow 1$  //  $n_b$ : number of row/column blocks, making  $n_b \times n_b$  grid of blocks.
3 else if  $r \leq 2/\sqrt{3}$  then  $n_b \leftarrow 2$ 
4 else  $n_b \leftarrow \lceil 2r \rceil$ 
5  $b \leftarrow 1 + \lfloor (m-1)/n_b \rfloor$  // Size of each block is at most  $b \times b$ 
6  $\ell \leftarrow 0$  // Accumulates log-abs-determinant of diagonal blocks
7  $\sigma \leftarrow 1$  // Keeps track of the parity of matrix

// Allocate memory for block matrices
8 Allocate memory for  $b \times b$  matrix  $\mathbf{A}$ 
9 if  $n_b > 1$  then Allocate memory for  $b \times b$  matrices  $\mathbf{B}, \mathbf{C}$ 
10 if  $n_b > 2$  then Allocate memory for  $b \times b$  matrix  $\mathbf{S}$ 

// Create scratchpad space on disk, large enough to store  $n_b(n_b - 1) - 1$  blocks
11 if  $n_b > 2$  then Allocate empty file of the size  $(m(m-b) - b^2)\beta$  bytes

// Recursive iterations over diagonal blocks
12 for  $k = 1$  to  $n_b$  do
13   if  $k = 1$  then  $\mathbf{A} \leftarrow \mathbf{M}_{kk}$  // Load from input array on disk
14    $\mathbf{A} \leftarrow \text{PLU}$  // In-place LU decomposition with pivoting (written to  $\mathbf{A}$ )
15    $\ell \leftarrow \ell + \text{logabsdet}(\mathbf{U})$ 
16    $\sigma \leftarrow \sigma \text{sgn}(\mathbf{P}) \text{sgn}(\mathbf{U})$ 
17   if  $k < n_b$  then
     // Iterate over row of blocks from bottom upward
18     for  $i = n_b$  to  $k + 1$  step  $-1$  do
19        $\mathbf{C} \leftarrow \mathbf{M}_{ik}^T$  // Load from disk (from input array if  $k = 1$  or from scratchpad if  $k > 1$ )
20        $\mathbf{C} \leftarrow \mathbf{U}^{-T}\mathbf{C}$  // Solve upper triangular system in-place

       // Iterate over column of blocks in alternating directions per row
21       if  $i - k$  is even then  $(j_{\text{start}}, j_{\text{end}}) \leftarrow (k + 1, n_b)$ 
22       else  $(j_{\text{start}}, j_{\text{end}}) \leftarrow (n_b, k + 1)$ 
23       for  $j = j_{\text{start}}$  to  $j_{\text{end}}$  step  $(-1)^{i-k}$  do
         // Load  $\mathbf{B}$  from disk (input array if  $k = 1$  and  $i = n_b$ , otherwise from scratchpad)
24         if  $i = n_b$  or  $j \neq j_{\text{start}}$  then  $\mathbf{B} \leftarrow \mathbf{M}_{kj}$ 
25         if  $i = n_b$  then
26            $\mathbf{B} \leftarrow \mathbf{L}^{-1}\mathbf{P}^T\mathbf{B}$  // Solve lower triangular system in-place
27           if  $n_b - k > 2$  or  $j \neq j_{\text{end}}$  then  $\mathbf{M}_{kj} \leftarrow \mathbf{B}$  // Write to disk on scratchpad
28         if  $i = k + 1$  and  $j = k + 1$  then
29            $\mathbf{A} \leftarrow \mathbf{M}_{ij}$  // Load from disk (input array if  $k = 1$  or scratchpad if  $k > 1$ )
30            $\mathbf{A} \leftarrow \mathbf{A} - \mathbf{C}^T\mathbf{B}$  // Compute Schur complement
31         else
32            $\mathbf{S} \leftarrow \mathbf{M}_{ij}$  // Load from disk (input array if  $k = 1$  or scratchpad if  $k > 1$ )
33            $\mathbf{S} \leftarrow \mathbf{S} - \mathbf{C}^T\mathbf{B}$  // Compute Schur complement
34            $\mathbf{M}_{ij} \leftarrow \mathbf{S}$  // Write to disk on scratchpad

35 return  $\ell, \sigma$ 

```

Algorithm C.2: MEMDET: Constrained-Memory Comp. of Log-Det (Case II: *Symmetric Matrix*)

Input : Symmetric matrix \mathbf{M} of size $m \times m$, // stored on disk, may not be loaded on memory
Maximum memory c in bytes

Output : $\pi := (\pi_q)_{q=1}^m$: a permutation of $\{1, \dots, m\}$ // permutations induced by LDL decomposition
 $\ell := (\ell_q)_{q=1}^m$: $\ell_q := \log_{\text{abs}} \det(\mathbf{M}_{[\mathcal{I}_q, \mathcal{I}_q]})$ with the index set $\mathcal{I}_q := (\pi_1, \dots, \pi_q)$ // $\log |\det(\cdot)|$
 $\sigma := (\sigma_q)_{q=1}^m$: $\sigma_q := \text{sgn}(\det(\mathbf{M}_{[\mathcal{I}_q, \mathcal{I}_q]})$ // Sign of $\det(\cdot)$

1 $r \leftarrow m\sqrt{\beta/c}$ // β : number of bytes per floating-point

2 **if** $r \leq 1$ **then** $n_b \leftarrow 1$ // n_b : number of row/column blocks, making $n_b \times n_b$ grid of blocks.

3 **else if** $r \leq 2/\sqrt{3}$ **then** $n_b \leftarrow 2$ **else** $n_b \leftarrow \lceil 2r \rceil$

4 $b \leftarrow 1 + \lfloor (m-1)/n_b \rfloor$ // Size of each block is at most $b \times b$

5 Initialize arrays $\mathbf{d} \in \mathbb{R}^m$ and $\pi \in \{1, \dots, m\}^m$ // Hold diagonals and permutations, respectively

// Allocate memory for block matrices

6 Allocate memory for $b \times b$ matrix \mathbf{A}

7 **if** $n_b > 1$ **then** Allocate memory for $b \times b$ matrices \mathbf{B}, \mathbf{C}

8 **if** $n_b > 2$ **then** Allocate memory for $b \times b$ matrix \mathbf{S}

9 **if** $n_b > 1$ **then** Define pointers $\mathbf{B}_*, \mathbf{C}_*$ // Used for swapping memory; $(\mathbf{B}_*, \mathbf{C}_*)$ will refer to (\mathbf{B}, \mathbf{C}) or (\mathbf{C}, \mathbf{B})

// Create scratchpad space on disk, large enough to store $n_b(n_b+1)/2 - 4$ blocks

10 **if** $n_b > 2$ **then** Allocate empty file of the size $(m(m+b)/2 - 4b^2)\beta$ bytes

// Recursive iterations over diagonal blocks

11 **for** $k = 1$ **to** n_b **do**

12 **if** $k = 1$ **then** $\mathbf{A} \leftarrow \mathbf{M}_{kk}$ // Load from input array on disk

13 $\mathbf{A} \leftarrow \text{PLDL}^\top \mathbf{P}^\top$ // In-place LDL^\top decomposition with pivoting (written to \mathbf{A})

14 $\mathbf{d}_{[1+(k-1)b:kb]} \leftarrow \text{diag}(\mathbf{D})$ // Accumulate diagonals of \mathbf{D} to \mathbf{d}

15 $\pi_{[1+(k-1)b:kb]} \leftarrow (k-1)b + \text{permutation}(\mathbf{P})$ // Accumulate permutation indices

16 **if** $k < n_b$ **then**

// Iterate over column of blocks backward (right to left)

17 **for** $j = n_b$ **to** $k+1$ **step** -1 **do**

18 **if** $n_b - j$ is even **then** $(\mathbf{B}_*, \mathbf{C}_*) = (\mathbf{B}, \mathbf{C})$ **else** $(\mathbf{B}_*, \mathbf{C}_*) = (\mathbf{C}, \mathbf{B})$ // swap \mathbf{B} and \mathbf{C} memories

19 **if** $j = n_b$ **then**

20 $\mathbf{B}_* \leftarrow \mathbf{M}_{kj}$ // Load from disk (input array if $k = 1$ or from scratchpad if $k > 1$)

21 $\mathbf{B}_* \leftarrow \mathbf{L}^{-1} \mathbf{P}^\top \mathbf{B}_*$ // Solve lower-triangular system in-place

22 $\mathbf{C} \leftarrow \mathbf{B}_*$ // Deep copy of the memory pointed by \mathbf{B}_* to memory pointed by \mathbf{C}_*

23 $\mathbf{B}_* \leftarrow \mathbf{D}^{-1} \mathbf{B}_*$

// Processing order of rows: first process row j , then from row $k+1$ downward to $j-1$

24 $\mathcal{R} \leftarrow (j, k+1, k+2, \dots, j-2, j-1)$

25 **for** $i = \mathcal{R}(1)$ **to** $\mathcal{R}(j-k)$ **do**

26 **if** $i \neq j$ **then** $\mathbf{C}_* \leftarrow \mathbf{M}_{ki}$ // Load disk (input array if $k = 1, j = n_b$, otherwise scratchpad)

27 **if** $j = n_b$ **then**

28 $\mathbf{C}_* \leftarrow \mathbf{L}^{-1} \mathbf{P}^\top \mathbf{C}_*$ // Solve lower triangular system in-place

29 **if** $n_b > 2$ **and** $i < j-1$ **then** $\mathbf{M}_{ki} \leftarrow \mathbf{C}_*$ // Write to disk on scratchpad

30 **if** $i = k+1$ **and** $j = k+1$ **then**

31 $\mathbf{A} \leftarrow \mathbf{M}_{ij}$ // Load from disk (input array if $k = 1$ or scratchpad if $k > 1$)

32 $\mathbf{A} \leftarrow \mathbf{A} - \mathbf{C}_*^\top \mathbf{B}_*$ // Compute Schur complement

33 **else**

34 $\mathbf{S} \leftarrow \mathbf{M}_{ij}$ // Load from disk (input array if $k = 1$ or scratchpad if $k > 1$)

35 $\mathbf{S} \leftarrow \mathbf{S} - \mathbf{C}_*^\top \mathbf{B}_*$ // Compute Schur complement

36 $\mathbf{M}_{ij} \leftarrow \mathbf{S}$ // Write to disk on scratchpad

37 $(\ell_0, \sigma_0) \leftarrow (0, 1)$

38 **for** $q = 1$ **to** m **do** $(\ell_q, \sigma_q) \leftarrow (\ell_{q-1} + \log(|d_q|), \sigma_{q-1} \text{sgn}(d_q))$ // d_q is the q -th element of \mathbf{d}

39 **return** π, ℓ, σ

Algorithm C.3: MEMDET: Constrained-Memory Comp. of Log-Det (Case III: *Symmetric Positive-Definite Matrix*)

Input : Symmetric positive-definite matrix \mathbf{M} of size $m \times m$, // stored on disk, not on memory
 Maximum memory c in bytes
Output : $\ell := (\ell_q)_{q=1}^m$; $\ell_q := \log\det(\mathbf{M}_{[q,q]})$

- 1 $r \leftarrow m\sqrt{\beta/c}$ // β : number of bytes per floating-point
- 2 **if** $r \leq 1$ **then** $n_b \leftarrow 1$ // n_b : number of row/column blocks, making $n_b \times n_b$ grid of blocks.
- 3 **else if** $r \leq 2/\sqrt{3}$ **then** $n_b \leftarrow 2$ **else** $n_b \leftarrow \lceil 2r \rceil$
- 4 $b \leftarrow 1 + \lfloor (m-1)/n_b \rfloor$ // Size of each block is at most $b \times b$
- 5 Initialize array $\mathbf{d} \in \mathbb{R}^m$ // Holds diagonals
- // Allocate memory for block matrices
- 6 Allocate memory for $b \times b$ matrix \mathbf{A}
- 7 **if** $n_b > 1$ **then** Allocate memory for $b \times b$ matrices \mathbf{B}, \mathbf{C}
- 8 **if** $n_b > 2$ **then** Allocate memory for $b \times b$ matrix \mathbf{S}
- 9 **if** $n_b > 1$ **then** Define pointers $\mathbf{B}_*, \mathbf{C}_*$ // Used for swapping memory; $(\mathbf{B}_*, \mathbf{C}_*)$ will refer to (\mathbf{B}, \mathbf{C}) or (\mathbf{C}, \mathbf{B})
- // Create scratchpad space on disk, large enough to store $n_b(n_b+1)/2 - 4$ blocks
- 10 **if** $n_b > 2$ **then** Allocate empty file of the size $(m(m+b)/2 - 4b^2)\beta$ bytes
- // Recursive iterations over diagonal blocks
- 11 **for** $k = 1$ **to** n_b **do**
- 12 **if** $k = 1$ **then** $\mathbf{A} \leftarrow \mathbf{M}_{kk}$ // Load from input array on disk
- 13 $\mathbf{A} \leftarrow \mathbf{L}\mathbf{L}^\top$ // In-place Cholesky decomposition (written to \mathbf{A})
- 14 $\mathbf{d}_{[1+(k-1)b:kb]} \leftarrow \text{diag}(\mathbf{L})$ // Accumulate diagonals of \mathbf{L} to \mathbf{d}
- 15 **if** $k < n_b$ **then**
- // Iterate over column of blocks backward (right to left)
- 16 **for** $j = n_b$ **to** $k+1$ **step** -1 **do**
- 17 **if** $n_b - j$ **is even** **then** $\mathbf{B}_* = \mathbf{B}$ **else** $\mathbf{B}_* = \mathbf{C}$ // Alternate pointer \mathbf{B}_* to switch between \mathbf{B} and \mathbf{C}
- 18 **if** $j = n_b$ **then**
- 19 $\mathbf{B}_* \leftarrow \mathbf{M}_{kj}$ // Load from disk (input array if $k = 1$ or from scratchpad if $k > 1$)
- 20 $\mathbf{B}_* \leftarrow \mathbf{L}^{-1}\mathbf{B}_*$ // Solve lower-triangular system in-place
- // Processing order of rows: first process row j , then from row $k+1$ downward to $j-1$
- 21 $\mathcal{R} \leftarrow (j, k+1, k+2, \dots, j-2, j-1)$
- 22 **for** $i = \mathcal{R}(1)$ **to** $\mathcal{R}(j-k)$ **do**
- 23 **if** $i = j$ **then** $\mathbf{C}_* = \mathbf{B}_*$ // Shallow copy of pointer \mathbf{C}_* pointing to \mathbf{B}_*
- 24 **else**
- 25 **if** $n_b - j$ **is even** **then** $\mathbf{C}_* = \mathbf{C}$ **else** $\mathbf{C}_* = \mathbf{B}$ // Alternate pointer \mathbf{C}_* between \mathbf{C} and \mathbf{B}
- 26 $\mathbf{C}_* \leftarrow \mathbf{M}_{ki}$ // Load \mathbf{C}_* from disk (input array if $k = 1, j = n_b$, otherwise scratchpad)
- 27 **if** $j = n_b$ **then**
- 28 $\mathbf{C}_* \leftarrow \mathbf{L}^{-1}\mathbf{C}_*$ // Solve lower triangular system in-place
- 29 **if** $n_b > 2$ **and** $i < j-1$ **then** $\mathbf{M}_{ki} \leftarrow \mathbf{C}_*$ // Write to disk on scratchpad
- 30 **if** $i = k+1$ **and** $j = k+1$ **then**
- 31 $\mathbf{A} \leftarrow \mathbf{M}_{ij}$ // Load from disk (input array if $k = 1$ or scratchpad if $k > 1$)
- 32 $\mathbf{A} \leftarrow \mathbf{A} - \mathbf{C}_*^\top \mathbf{B}_*$ // Compute Schur complement
- 33 **else**
- 34 $\mathbf{S} \leftarrow \mathbf{M}_{ij}$ // Load from disk (input array if $k = 1$ or scratchpad if $k > 1$)
- 35 $\mathbf{S} \leftarrow \mathbf{S} - \mathbf{C}_*^\top \mathbf{B}_*$ // Compute Schur complement
- 36 $\mathbf{M}_{ij} \leftarrow \mathbf{S}$ // Write to disk on scratchpad
- 37 $\ell_0 \leftarrow 0$
- 38 **for** $q = 1$ **to** m **do** $\ell_q \leftarrow \ell_{q-1} + 2\log(d_q)$ // d_q is the q -th element of \mathbf{d}
- 39 **return** ℓ

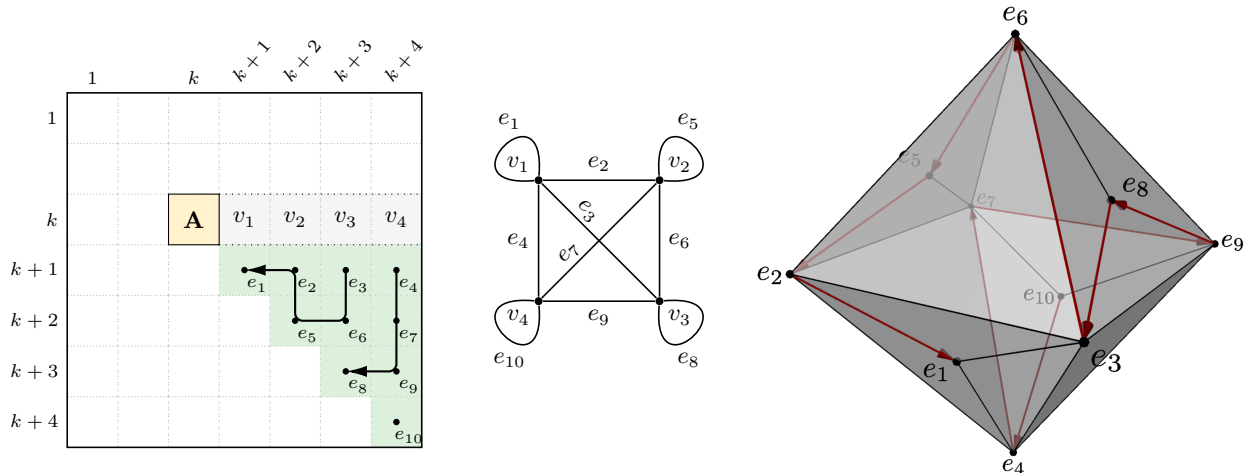


Figure D.1: *Left*: Example of the processing order of blocks for a symmetric matrix at the k -th hierarchical step. In this step, to process $\mathbf{S} \leftarrow \mathbf{M}_{ij}$, the memory blocks \mathbf{B} and \mathbf{C} are selected from the set $V = \{v_1, v_2, v_3, v_4\}$. *Middle*: The corresponding complete graph $G(V, E)$. *Right*: The corresponding line graph $L(G)$, with one possible Hamiltonian path highlighted in red, starting from the node e_{10} and ending at the node e_1 .

Given that G is complete and therefore Hamiltonian, it follows that its line graph $L(G)$ is also Hamiltonian. This implies the existence of at least one (but possibly many) Hamiltonian paths. Crucially, all Hamiltonian paths in $L(G)$ have the same length. Consequently, any sequence of blocks derived from a Hamiltonian path constitutes an optimal solution to our problem. Thus, the block sequence presented in Figure 1 is equivalent in optimality to any other sequence obtainable from a Hamiltonian path.

The same problem can be formulated for the block LU decomposition, with the modification that G is a complete and balanced bipartite graph $G(V, V, E)$; however, the same logic and conclusion follow.

Appendix E Complexity and Performance Analysis of MEMDET

E.1 Computational Complexity

Table E.1 provides a detailed breakdown of the computational complexity of MEMDET for generic matrices (second column, using LU decomposition) and symmetric matrices (third column, using LDL or Cholesky decomposition). The operations are categorized into matrix decomposition, solving triangular systems, and matrix multiplications used to form Schur complements. Each operation's complexity is given in terms of the number of times it is performed and the FLOP count per operation. In this analysis, a single floating-point fused multiply-add (FMA) operation is counted as one FLOP. The table reports a single complexity column for symmetric matrices, covering both LDL and Cholesky decompositions; while LDL involves additional operations such as row permutations and handling the diagonal matrix \mathbf{D} , these steps are excluded from the FLOP count, as their computational cost is negligible compared to the dominant terms.

The complexity of each operation is given by the number of times it is performed (a function of n_b) multiplied by the FLOP count per operation (a function of the block size b). Substituting $b = m/n_b$ into these expressions, the total complexity, obtained by summing across all operations, simplifies such that n_b cancels out, as shown in the last row of Table E.1. Thus, the total computational complexity of MEMDET is independent of the number of blocks n_b , and is identical to that of conventional factorization algorithms where $n_b = 1$.

Although the total computational cost remains the same, the contribution of individual operations shifts as n_b increases. When $n_b = 1$, the entire computation consists solely of a matrix decomposition. As n_b increases, the decomposition cost decreases while additional operations, such as solving triangular systems and matrix multiplications, account for a larger fraction of the total complexity. At the extreme case of $n_b = m$, the

Table E.1: Breakdown of computational complexity for MEMDET. The table presents the number of operations performed and the FLOP count per operation for generic matrices (LU decomposition) and symmetric matrices (LDL or Cholesky decomposition). The last row shows the total complexity, which remains independent of the number of blocks n_b .

Operation	Generic Matrix		Symmetric (Positive-Definite) Matrix	
	Num. Operations	FLOPs per Operation	Num. Operations	FLOPs per Operation
Matrix Decomposition	n_b	$\frac{1}{3}b^3 - \frac{1}{2}b^2 + \frac{1}{6}b$	n_b	$\frac{1}{6}b^3 - \frac{1}{4}b^2 + \frac{1}{12}b$
Solve Lower Triangular System	$\frac{1}{2}n_b^2 - \frac{1}{2}n_b$	$\frac{1}{2}b^3 - \frac{1}{2}b^2$	$\frac{1}{2}n_b^2 - \frac{1}{2}n_b$	$\frac{1}{2}b^3 - \frac{1}{2}b^2$
Solve Upper Triangular System	$\frac{1}{2}n_b^2 - \frac{1}{2}n_b$	$\frac{1}{2}b^3 - \frac{1}{2}b^2$		
Full Matrix Multiplication	$\frac{1}{3}n_b^3 - \frac{1}{2}n_b^2 + \frac{1}{6}n_b$	b^3	$\frac{1}{6}n_b^3 - \frac{1}{2}n_b^2 + \frac{1}{3}n_b$	b^3
Gramian Matrix Multiplication			$\frac{1}{2}n_b^2 - \frac{1}{2}n_b$	$\frac{1}{2}b^3$
Total Complexity		$\frac{1}{3}m^3 - \frac{1}{2}m^2 + \frac{1}{6}m$		$\frac{1}{6}m^3 - \frac{1}{4}m^2 + \frac{1}{12}m$

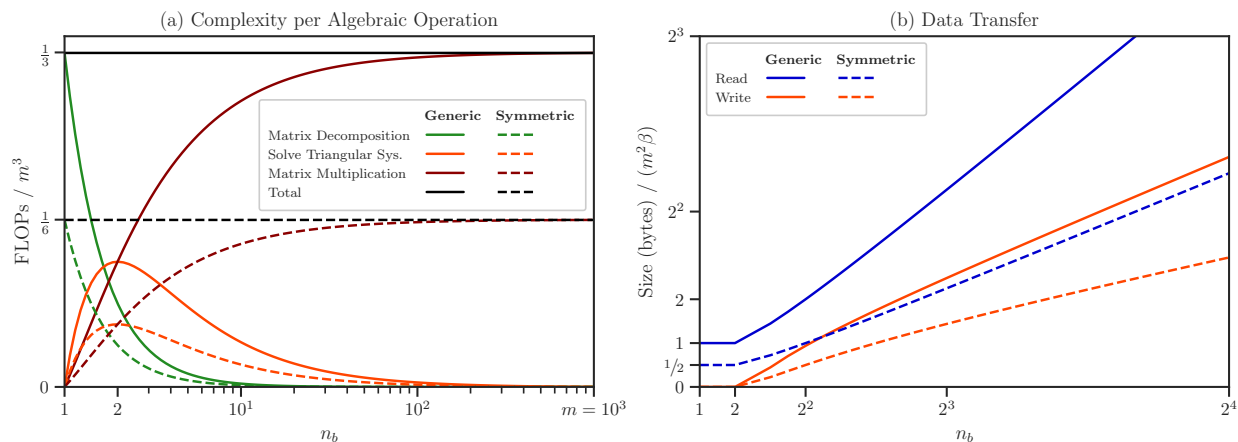


Figure E.1: Theoretical computational complexity of MEMDET as a function of the number of blocks n_b . The left panel shows the contributions of matrix decomposition, solving triangular systems, and matrix multiplication to the total complexity. The black curve represents the total computational cost, which remains constant, while the colored curves illustrate how the workload shifts across operations as n_b increases. The right panel displays the total data transfer volume (normalized by the original matrix size) for different n_b , highlighting the increasing cost of disk I/O as the number of blocks grows.

algorithm consists primarily of matrix multiplications. This transition is illustrated in Figure E.1 (left panel), where the contributions of matrix decomposition, triangular system solving, and matrix multiplication are plotted as functions of n_b . The total computational complexity, shown as the black curve, remains constant, while the distribution of work among different operations shifts as n_b increases.

E.2 Data Transfer and Memory Considerations

While the total FLOP count is independent of n_b , the number of data transfers between memory and disk increases with the number of blocks. Table E.2 summarizes the number of blocks read from disk to memory and written back to disk, as a function of n_b . The actual volume of transferred data is obtained by multiplying the number of blocks by the block size, $b^2\beta$, where β represents the number of bytes per floating point. The right panel of Figure E.1 illustrates the total data transfer volume relative to the original matrix size.

Table E.2: Number of blocks transferred between disk and memory during MEMDET execution. The total data transfer volume is obtained by multiplying the number of transferred blocks by the block size, $b^2\beta$ bytes, where $b = m/n_b$. Read operations occur in all cases, while write operations to the scratchpad are only required for $n_b > 2$.

Operation	Generic Matrix	Symmetric Matrix
Read	$\frac{2}{3}n_b^3 - n_b^2 + \frac{4}{3}n_b$	$\frac{1}{3}n_b^3 - \frac{1}{2}n_b^2 + \frac{7}{6}n_b$
Write	$\begin{cases} 0, & n_b \leq 2 \\ \frac{1}{3}n_b^3 - \frac{4}{3}n_b - 1, & n_b > 2 \end{cases}$	$\begin{cases} 0, & n_b \leq 2 \\ \frac{1}{6}n_b^3 + \frac{1}{2}n_b^2 - \frac{11}{3}n_b + 4, & n_b > 2 \end{cases}$

Table E.3: Number of concurrent blocks that must be allocated in memory and the total number of blocks allocated on disk during MEMDET execution. The total required memory and disk space are obtained by multiplying the number of allocated blocks by the block size, $b^2\beta$ bytes. While the number of concurrent memory-resident blocks remains fixed, the total number of blocks allocated on disk increases with $n_b > 2$.

Hardware	Generic Matrix	Symmetric Matrix
Memory	3 or 4	3 or 4
Scratchpad	$\begin{cases} 0, & n_b \leq 2 \\ n_b^2 - n_b - 1, & n_b > 2 \end{cases}$	$\begin{cases} 0, & n_b \leq 2 \\ \frac{1}{2}n_b^2 + \frac{1}{2}n_b - 4, & n_b > 2 \end{cases}$

For $n_b \leq 2$, the entire computation can often fit in memory, avoiding disk I/O, requiring no scratchpad space. However, for $n_b > 2$, the data transfer overhead increases approximately as $\mathcal{O}(n_b^2)$, meaning that choosing an excessively high n_b introduces unnecessary I/O costs. Despite this, the hierarchical design of MEMDET efficiently schedules block transfers, mitigating excessive data movement.

Table E.3 provides an analysis of the required memory and scratchpad space. The number of blocks stored in memory and on disk is determined by n_b , with the actual space usage obtained by multiplying the number of blocks by the block size. By adjusting n_b , MEMDET can be configured to run within any given memory constraint, making it adaptable to systems with limited memory.

E.3 Empirical Performance Evaluation

To validate the theoretical complexity and memory analysis, we conducted empirical evaluations on SPD matrices of various sizes, ranging from $m = 2^{10}$ to 2^{16} . The largest matrix tested was chosen to match the memory capacity of a 64 GB system, allowing for a direct comparison between MEMDET and conventional algorithms. For each matrix size, the algorithm was executed with different numbers of blocks, $n_b = 1, 2, \dots, 8$, where $n_b = 1$ corresponds to a standard full-matrix decomposition with the entire matrix loaded into memory. Each experiment was repeated 10 times, and the mean and standard deviation of the profiling measures are reported.

Figure E.2 presents the experimental results. The left panel shows peak memory allocation, measured using a memory profiling tool, which precisely matches the theoretical predictions. As expected, when $n_b = 1$, the required memory equals the original matrix size, while increasing n_b reduces the memory footprint. The middle and right panels display the measured process time as functions of n_b and m , respectively. At large m , the difference in process time across varying n_b diminishes, indicating that the increase in data transfer cost does not significantly impact overall runtime.

To further analyze this effect, Figure E.3 decomposes the process time into computation time and data transfer time. At small m , the runtime is dominated by disk I/O, but as m increases, computation time becomes the dominant factor. This confirms that for sufficiently large matrices, the performance of MEMDET approaches that of conventional in-memory methods.

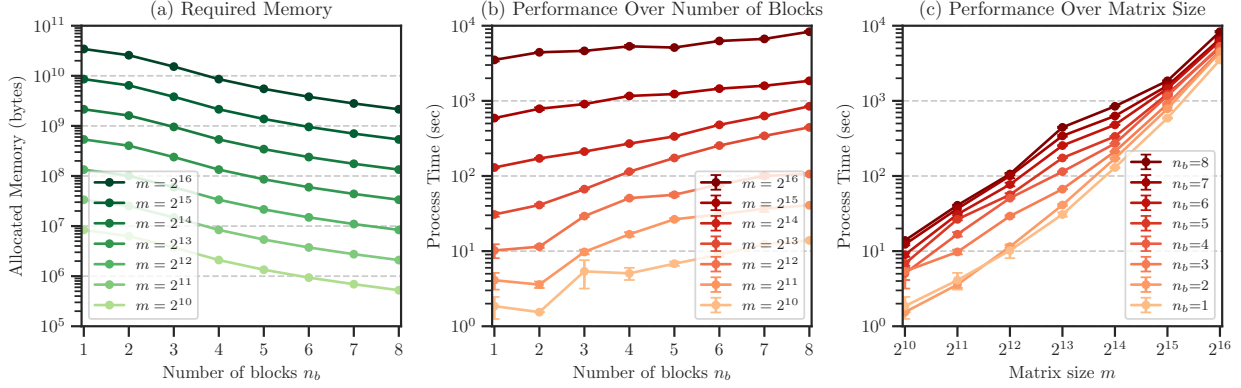


Figure E.2: Peak memory allocation (a) and CPU processing time (b, c) for MEMDET on symmetric positive-definite matrices of size $m = 2^{10}, \dots, 2^{16}$, using Algorithm C.3. The matrices were processed using an $n_b \times n_b$ grid of matrix blocks, where $n_b = 1, 2, \dots, 8$.

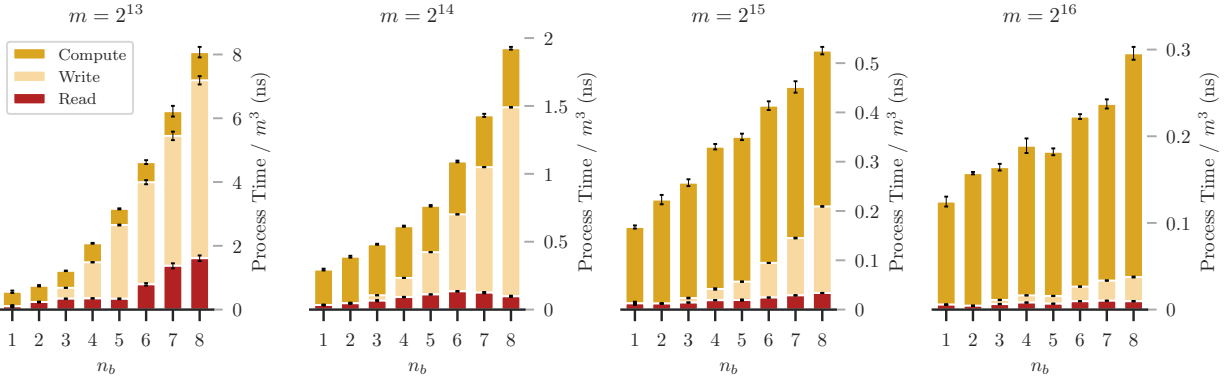


Figure E.3: Breakdown of MEMDET runtime (using Algorithm C.3) into computation and data transfer times, normalized by m^3 , for $m = 2^{13}, \dots, 2^{16}$. The total process time consists of reading from disk to memory (maroon), writing from memory to disk (light tan), and computation (ochre).

E.4 Concluding Remarks of Performance Analysis

MEMDET maintains the same computational complexity as conventional factorization methods while distributing computations across blocks. The total FLOP count remains unchanged, but increasing n_b shifts the workload between operations (i.e., from matrix decompositions to matrix multiplications). However, increasing n_b also increases data transfer overhead, requiring a balance between reducing memory usage and minimizing disk I/O.

The hierarchical scheduling of block operations optimizes memory usage while limiting unnecessary data movement, ensuring that MEMDET remains efficient under constrained memory conditions. By allowing users to specify a memory limit, MEMDET enables the processing of arbitrarily large matrices on systems with any limited memory size.

For large-scale applications, where conventional methods exceed memory capacity, MEMDET provides a practical alternative. The experiments confirm that while data transfer overhead exists, it does not significantly impact runtime at large m , making MEMDET a viable solution for large-matrix computations on standard hardware.

Appendix F Background Material for Neural Scaling Laws

The noiseless result from (Li et al., 2023) that we require is contingent upon the following assumptions:

Assumption F.1 (Eigenvalue Decay). There exists a $\beta > 1$ and constants $c_\beta, C_\beta > 0$ such that

$$c_\beta i^{-\beta} \leq \lambda_i \leq C_\beta i^{-\beta}, \quad (\text{F.1})$$

where the λ_i are eigenvalues of the kernel $k : \mathcal{X} \times \mathcal{X} \rightarrow \mathbb{R}$ under the decomposition guaranteed by Mercer's Theorem:

$$\kappa(x, x') = \sum_{i=1}^{\infty} \lambda_i e_i(x) e_i(x'). \quad (\text{F.2})$$

We need to define an embedding index associated to certain interpolation spaces that arise as the range of fractional powers of integral operators. In order to do so, we define the integral operator $T : L^2 \rightarrow L^2$ that acts as the natural embedding of a RKHS \mathcal{H} associated with our kernel κ , precomposed with its adjoint. That is, T is the integral operator given by

$$(Tf)(x) = \int_{\mathcal{X}} \kappa(x, x') f(x') d\mu(x'),$$

where μ is the marginal distribution on \mathcal{X} of ρ , the source distribution on $(\mathcal{X} \times \mathcal{Y})$ underlying the dataset. The operator T can be decomposed by the spectral theorem of compact self-adjoint operators via

$$T = \sum_{i=1}^{\infty} \lambda_i \langle \cdot, e_i \rangle_{L^2} e_i. \quad (\text{F.3})$$

For $s \geq 0$, this lets us define the fractional powers $T^s : L^2 \rightarrow L^2$ of the operator T to satisfy

$$T^s(f) = \sum_{i=1}^{\infty} \lambda_i^s \langle f, e_i \rangle_{L^2} e_i. \quad (\text{F.4})$$

The interpolation space $[\mathcal{H}]^s$ associated to $T^{s/2}$ can then be defined as

$$[\mathcal{H}]^s = \text{Range}(T^{s/2}) = \left\{ \sum_{i=1}^{\infty} a_i \lambda_i^{\frac{s}{2}} e_i \mid \sum_{i=1}^{\infty} a_i^2 < \infty \right\} \subset L^2. \quad (\text{F.5})$$

We now say that \mathcal{H} has an embedding property of order $\alpha \in (0, 1]$ if $[\mathcal{H}]^\alpha$ can be continuously embedded into L^∞ . Define then the operator norm, which has the form (see (Fischer & Steinwart, 2020))

$$\|[\mathcal{H}]^s \hookrightarrow L^\infty\| = \text{ess sup}_{x \in \mathcal{X}, \mu} \sum_{i=1}^{\infty} \lambda_i^\alpha e_i(x)^2.$$

We now have the following assumption on the embedding index, which is known to be satisfied if the eigenfunctions e_i are uniformly bounded (Steinwart et al., 2009).

Assumption F.2 (Embedding index). The embedding index $\alpha_0 = 1/\beta$, where β is the eigenvalue decay in (F.1), and α_0 is defined as

$$\alpha_0 = \inf \{ \alpha : \|[\mathcal{H}]^s \hookrightarrow L^\infty\| = M_\alpha < \infty \}$$

Finally, we have the following assumption on the smoothness of the source function $f_\rho^* = \mathbb{E}_\rho[y \mid x]$, which is a more precise characterization than requiring it to belong to some interpolation space.

Assumption F.3 (Source condition). There exists an $s > 0$ and a sequence $(a_i)_{i \geq 1}$ for which

$$f_\rho^* = \sum_{i=1}^{\infty} a_i \lambda_i^{\frac{s}{2}} i^{-\frac{1}{2}} e_i,$$

and $0 < c \leq |a_i| \leq C$ for some constants c, C .

These assumptions are required for the following theorem, taken from (Li et al., 2023).

Theorem F.1. *Under Assumptions F.1 to F.3, fix $s > 1$ and suppose that $\lambda \asymp n^{-\theta}$ for $\theta \geq \beta$. Then*

$$\text{Bias}^2 = E(n) = \mathcal{O}_{\mathbb{P}}^{\text{poly}}(n^{-\min(s,2)\beta}).$$

Appendix G Proofs of Lemma 1 and Proposition 1

Proof of Lemma 1. Fix $\alpha > 0$ and write $\mathbf{K}_n^\alpha = \mathbf{K}_n + \alpha \text{Id}_{n \times n}$. In block form, \mathbf{K}_n^α contains \mathbf{K}_{n-1}^α according to

$$\mathbf{K}_n^\alpha = \begin{bmatrix} \mathbf{K}_{n-1}^\alpha & \kappa(\mathbf{x}_{n-1}, x_n) \\ \kappa(\mathbf{x}_{n-1}, x_n)^\top & \kappa(x_n, x_n) + \alpha \end{bmatrix},$$

where $\kappa(\mathbf{x}_{n-1}, x_n) = (\kappa(x_i, x_n))_{i=1}^{n-1} \in \mathbb{R}^{nd \times d}$. Consequently, since \mathbf{K}_n^α and \mathbf{K}_{n-1}^α are both positive-definite, their determinants differ by the Schur determinant:

$$\det(\mathbf{K}_n^\alpha) = \det(\mathbf{K}_{n-1}^\alpha) \det(\kappa(x_n, x_n) + \alpha - \kappa(\mathbf{x}_{n-1}, x_n)^\top [\mathbf{K}_{n-1}^\alpha]^{-1} \kappa(\mathbf{x}_{n-1}, x_n)).$$

Combining the Sylvester rank inequality with Corollary 20 from (Ameli & Shadden, 2023), we take $\alpha \downarrow 0$ and observe that

$$\text{pdet}(\mathbf{K}_n) \leq \text{pdet}(\mathbf{K}_{n-1}) \text{pdet}(\text{Cov}(f(x_n) \mid f(x_i) = 0 \text{ for } i = 1, \dots, n-1)). \quad (\text{G.1})$$

This lets us apply the AM-GM inequality and then bound the Frobenius norm in terms of the nuclear norm to obtain

$$\begin{aligned} \frac{\text{pdet}(\mathbf{K}_n)}{\text{pdet}(\mathbf{K}_{n-1})} &\leq \text{pdet}(\text{Cov}(f(x_n) \mid f(x_i) = 0 \text{ for } i = 1, \dots, n-1)) = \prod_{j=1}^r \lambda_j \leq r^{-\frac{r}{2}} \left(\sum_{j=1}^r \lambda_j^2 \right)^{\frac{r}{2}} \\ &\leq r^{-\frac{r}{2}} \text{trace}(\text{Cov}(f(x_n) \mid f(x_i) = 0 \text{ for } i = 1, \dots, n-1)^r) \\ &\leq \left(\frac{d}{r} \right)^{r/2} E(n)^r, \end{aligned}$$

where the λ_j are the non-zero eigenvalues of the covariance matrix, and r is its rank. □

Proof of Proposition 1. From equation (3),

$$\begin{aligned} \log \det(\mathbf{K}_n) - \log \det(\mathbf{K}_{n-1}) &= \log C - \nu \log n + \log[1 + o_p(1)] \\ &= \log C - \nu \log n + o_p(1), \end{aligned} \quad (\text{G.2})$$

and so

$$\log \det(\mathbf{K}_n) - \log \det(\mathbf{K}_1) = (n-1) \log C - \nu \log(n!) + o_p(n).$$

Letting $c_0 := \log C - \log \det(\mathbf{K}_1)$ and dividing by n implies the first result. For the second result, we replace the $o_p(1)$ term in (G.2) with δ_{n-1} . Consequently,

$$\frac{n}{\sqrt{n-1}} \left[L_n - L_1 - \left(1 - \frac{1}{n}\right) c_0 + \nu \frac{\log(n!)}{n} \right] = (n-1)^{-1/2} \sum_{i=1}^{n-1} \delta_i,$$

and from (Billingsley, 1961), $(n-1)^{-1/2} \sum_{i=1}^{n-1} \delta_i$ converges weakly to a normal random variable with zero mean and variance $\sigma^2 = \mathbb{E}[\delta_1^2]$. □

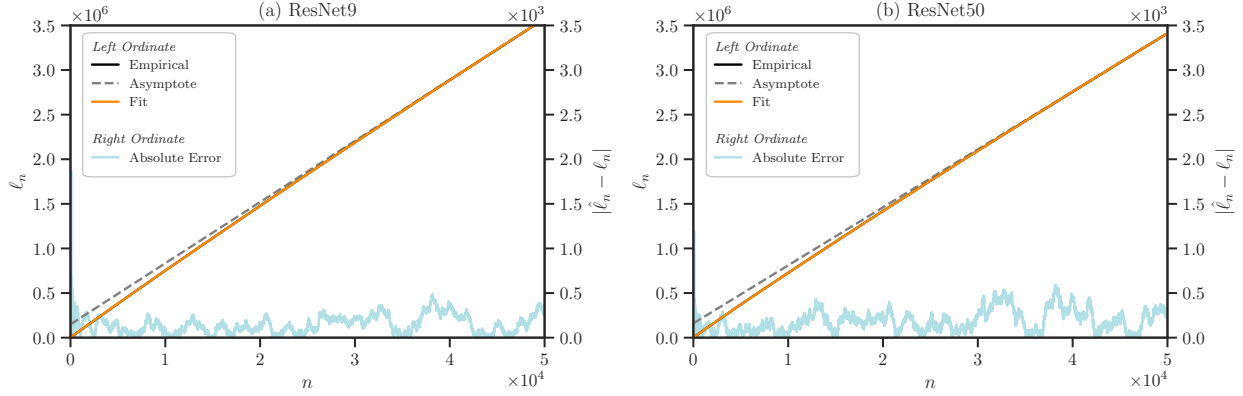


Figure H.1: Log-determinant ℓ_n for $n = 1, \dots, 50,000$, corresponding to $m \times m$ NTK submatrices where $m = nd$ and $d = 10$, from ResNet9 (a) and ResNet50 (b) trained on CIFAR-10 with 50,000 datapoints. Values are computed using MEMDET (Algorithm C.2) with LDL decomposition (black curves, overlaid by colored curves). The orange curves represent theoretical fits based on the parametrization derived in Algorithm 1. Fitting is performed globally over the entire interval $(n_0, n) = (1, 5 \times 10^4)$, demonstrating the accuracy of the theoretical model. The blue curve, corresponding to the right axis (scaled to one-thousandth of the left axis), shows the absolute error.

Appendix H Derivation of FLODANCE Parameterization

Letting $\nu_n = \nu_0 + \sum_{i=1}^q \nu_i n^{-i}$, Proposition 1 implies that, asymptotically in n ,

$$L_n = L_1 + \left(1 - \frac{1}{n}\right) c_0 - \left(\nu_0 + \sum_{i=1}^q \frac{\nu_i}{n^i}\right) \frac{\log(n!)}{n} + \frac{\sqrt{n-1}}{n} \epsilon_n, \quad \epsilon_n \stackrel{\text{iid}}{\sim} \mathcal{N}(0, \sigma^2),$$

for some c_0, ν_0, \dots, ν_q and $\sigma > 0$. Rearranging, there is

$$\frac{n}{\sqrt{n-1}}(L_n - L_1) = \frac{n-1}{\sqrt{n-1}} c_0 - \left(\nu_0 + \sum_{i=1}^q \frac{\nu_i}{n^i}\right) \frac{\log(n!)}{\sqrt{n-1}} + \epsilon_n,$$

and equivalently,

$$y_n = c_0 x_{n,0} + \sum_{i=1}^{q+1} \nu_{i-1} x_{n,i} + \epsilon_n,$$

where

$$x_{n,0} = \sqrt{n-1}, \quad x_{n,i} = \frac{\log(n!)}{n^{i-1} \sqrt{n-1}}, \quad y_n = \frac{n}{\sqrt{n-1}}(L_n - L_1).$$

To validate the theoretical parameterization, we empirically compute the log-determinants of NTK submatrices of size $1, \dots, n$ from ResNet9 and ResNet50 trained on CIFAR-10, where $n = 50,000$. The log-determinants are computed using MEMDET (Algorithm C.2) with LDL decomposition. Figure H.1 presents the empirical results, where the black curves (overlaid by orange curves) represent the computed log-determinants, and the orange curves show the theoretical fits obtained using the parameterization in Algorithm 1. The fitting is performed globally over the entire interval, demonstrating the effectiveness of the theoretical model in capturing the log-determinant behavior. The near-perfect overlap between the curves in both cases highlights the accuracy of the fit, with errors remaining below 0.05% for most of the interval.

Appendix I Implementation and Reproducibility Guide

We developed a Python package `detkit`⁴ that implements the MEMDET algorithm and can be used to reproduce the numerical results of this paper. A minimalistic usage of the `detkit.memdet` function is shown in [Listing I.1](#), where the user can specify various parameters: the maximum memory limit (`max_mem`), the structure of the matrix via the `assume` argument—set to `gen` for generic matrices ([Algorithm C.1](#)), `sym` for symmetric matrices ([Algorithm C.2](#)), and `spd` for symmetric positive-definite matrices ([Algorithm C.3](#))—whether the data is provided in full or in its lower/upper triangular form (`triangle`), the arithmetic precision used during computation (`mixed_precision`), the location of scratchpad space on disk (`scratch_dir`), and enabling parallel data transfer between memory and disk (`parallel_io`).

Listing I.1: A minimalistic usage of `detkit` package. The function `memdet` computes $\log\text{absdet}(\mathbf{M})$ using the MEMDET algorithm.

```
# Install detkit with "pip install detkit"
from detkit import memdet
import zarr

5 # NTK matrix M on disk
M = zarr.open('filename.zarr', 'r')

# Compute logabsdet(M) and sgn(det(M)) with Algorithm C.2
# Assume M is symmetric and only its upper triangle part is referenced.
10 ld, sign, diag, perm, info = memdet(M, max_mem='32GB', assume='sym', triangle='u',
                                     overwrite=False, mixed_precision='float64',
                                     scratch_dir='/tmp', parallel_io='tensorstore',
                                     verbose=True, return_info=True, flops=True)
```

An example of utilizing FLODANCE is shown in [Listing I.2](#) using the `FitLogdet` class in `detkit`. A small subset of log-determinants from submatrices, computed in [Listing I.1](#), is used to extrapolate log-determinants of larger submatrices via [Algorithm 1](#).

We have also concurrently developed a separate high-performance Python package, `imate`,⁵ which implements stochastic Lanczos quadrature (SLQ), a randomized method for approximating the log-determinant at scale. This package is implemented with a C++/CUDA backend and supports execution on both CPU and multiple GPUs. [Listing I.3](#) demonstrates a minimalistic usage of the `imate.logdet` function.

⁴`detkit` is available for installation from PyPI (<https://pypi.org/project/detkit>), the documentation can be found at <https://ameli.github.io/detkit>, and the source code is available at <https://github.com/ameli/detkit>.

⁵`imate` is available for installation from PyPI (<https://pypi.org/project/imate>), the documentation can be found at <https://ameli.github.io/imate>, and the source code is available at <https://github.com/ameli/imate>.

Listing I.2: The class `FitLogdet` fits and extrapolates log-determinants using FLODANCE in [Algorithm 1](#).

```

import numpy as np
from detkit import FitLogdet

# Range of datapoints (n) and number of labels (d) for CIFAR-10
5 n, d = np.range(50000), 10

# Compute  $\ell_k := \log\text{absdet}(\mathbf{M}_{[:k:k]})$  for sub-matrices of the size  $k = 1, \dots, m = nd$ 
# Here, diag is an array of length  $m$  obtained from Listing I.1
ell = np.cumsum(np.log(np.abs(diag)))
10

# Keep every  $d$ -th element
ell = ell[(d-1)::d]

# Choose a fit interval, such as  $(n_0, n_s) = (10^2, 5 \times 10^3)$ 
15 n0, ns = 1e2, 5e3
fit_mask = (n > n0) & (n < ns)

# Fit using Algorithm 1 with 4-th order truncated Laurent series
flodet = FitLogdet(q=4)
20 flodet.fit(n[fit_mask], ell[fit_mask])

# Extrapolate in a larger interval, such as in  $(n_s, n) = (5 \times 10^3, 5 \times 10^4)$ 
n_eval = np.geomspace(ns, n)
ell_eval = flodet.eval(n_eval)

```

Listing I.3: A minimalistic usage of `imate` package. The function `logdet` computes $\log\det(\mathbf{M})$ using the stochastic Lanczos quadrature algorithm.

```

# Install imate with "pip install imate"
from imate import logdet
import numpy

5 # Number of detests (n) and labels (d)
n, d = 50000, 10

# NTK matrix  $\mathbf{M}$  on disk
M = numpy.memmap('filename.npy', mode='r', dtype='float32', shape=(n*d, n*d))
10

# Compute  $\log\det(\mathbf{M})$  using stochastic Lancos quadrature (SLQ) method
# Assume  $\mathbf{M}$  is symmetric.
ld, info = logdet(M, method='slq', min_num_samples=100, max_num_samples=200,
15     lanczos_degree=100, error_rtol=0.01, confidence_level=0.95,
     outlier_significance_level=0.001, orthogonalize=-1, num_threads=0,
     num_gpu_devices=0, gpu=True, verbose=True, return_info=True,
     plot=True)

```
